UNIVERSITAT POLITÈCNICA DE VALÈNCIA

UNIVERSITAT POLITÈCNICA DE VALÈNCIA

School of Industrial Engineering

Performance and durability optimization of a hydrogen multiple fuel cell system for heavy-duty transport applications

Master's Thesis

Master's Degree in Industrial Engineering

AUTHOR: Luengo Pérez-Hickman, Pablo

Tutor: Novella Rosa, Ricardo

Cotutor: López Juárez, Marcos

ACADEMIC YEAR: 2021/2022

ABSTRACT

The goal of this study is to examine the potential economic and environmental benefits of using FCs (FC) as the propulsion system of a heavy-duty vehicle. A modelling platform has been used to simulate HDFCV drive cycles that integrates control strategy optimisation algorithms, a modelling platform with independent FC, battery and electric motor models and a FC degradation model that can run in parallel during the simulation of drive cycles. An analysis of the multi-FC system is then performed to demonstrate the impact of FC-battery power split and dynamic strategies on the performance of the propulsion system and durability of the FC stack. At this point, a pilot route is implemented for the truck diary service in order to be able to carry out a total cost of ownership and a life cycle assessment study to show the evaluate the costa and environmental impact reduction potential of this technology in Europe 2022 and 2030 scenarios.

RESUMEN

El objetivo de este estudio es examinar los posibles beneficios económicos y medioambientales del uso de pilas de combustible (FC) como sistema de propulsión de un vehículo pesado. Se ha utilizado una plataforma de modelización para simular los ciclos de propulsión de un HDFCV que integra algoritmos de optimización de la estrategia de control, una plataforma de modelización con modelos independientes de FC, batería y motor eléctrico y un modelo de degradación de FC que puede ejecutarse en paralelo durante la simulación de los ciclos de propulsión. A continuación, se lleva a cabo un análisis del sistema multi-FC para demostrar el impacto de la división de energía FC-batería y las estrategias dinámicas en el rendimiento del sistema de propulsión y la durabilidad de la pila de FC. En este punto, se implementa una ruta piloto para el servicio diario de camiones con el fin de poder llevar a cabo un coste total de propiedad y un estudio de evaluación del ciclo de vida para mostrar la evaluación del potencial de reducción de costes e impacto medioambiental de esta tecnología en los escenarios de Europa 2022 y 2030.

RESUM

L'objectiu d'aquest estudi és examinar els beneficis econòmics i mediambientals possibles de l'ús de piles de combustible (FC) com a sistema de propulsió d'un vehicle pesant. S'ha fet servir una plataforma de modelització per simular els cicles de propulsió d'un HDFCV que integra algorismes d'optimització de l'estratègia de control, una plataforma de modelització amb models independents de FC, bateria i motor elèctric i un model de degradació de FC executar-se en paral·lel durant la simulació dels cicles de propulsió. A continuació, es fa una anàlisi del sistema multi-FC per demostrar l'impacte de la divisió d'energia FC-bateria i les estratègies dinàmiques en el rendiment del sistema de propulsió i la durabilitat de la pila de FC. En aquest punt, s'implementa una ruta pilot per al servei diari de camions per tal de poder dur a terme un cost total de propietat i un estudi d'avaluació del cicle de vida per mostrar l'avaluació del potencial de reducció de costos i impacte mediambiental d'aquesta tecnologia als escenaris d'Europa 2022 i 2030.

INDEX

Figure Index

TABLE INDEX

Symbols and Nomenclature

FC	Fuel Cell
FCV	Fuel Cell Vehicle
FCEV	Fuel Cell Electric Vehicle
FCET	Fuel Cell Electric Truck
FCREx	Fuel Cell Range Extender
BEV	Battery Electric Vehicle
BET	Battery Electric Truck
PEMFC	Proton Exchange Membrane Fuel Cell
AFC	Alkaline Fuel Cells
PAF	Phosphoric acid fuel cells
MCFC	Molten carbonate fuel cells
SOF	Solid oxide fuel cells
EU	Europe
H2	Hydrogen
GHG	Green House Gases
GWP	Global Warming Potential
CO2	Carbon Dioxide
NOX	Nitrogen oxides
SOX	Sulfur oxide
CH4	Methane
N20	Nitrous Oxide
HDV	Heavy Duty Vehicle
IEA	International Energy Agency
ICCT	International Council on Clean Transportation
DC	Direct Current
AC	Alternating Current
ORR	Oxygen Reduction Reactions
HOR	Hydrogen Oxidation Reactions
USD	United States dollar(s)
TCO	Total Cost of Ownership
LCA	Life Cycle Assessment
SoC	State of Charge
WLTC	World Harmonized Light-duty Vehicle Test Cycle
0D-1D	Cero Dimension- One Dimension
OC	Optimal Control
BoP	Balance of Plant
RH	Relative Humidity
PID	Process Identifier
ICE	Internal Combustion Engine
CI	Compressed Ignition
RC	Equivalent Electric Circuit
ECSA	Electrochemical surface area
EOL	End Of Life

1. INTRODUCTION

1.1. Context of the heavy-duty transport sector

Europe is one of the world's greatest emitters of greenhouse gases, and it plays a critical role in meeting the goal of limiting the worldwide average temperature increase to 1.5ºC with respect to pre-industrialization levels. The EU's transportation emissions have increased by 33% since 1990 and are continuing to rise. The largest emitter is light-duty vehicles, followed by heavy-duty vehicles, maritime navigation, and aircraft (*Figure 1*).

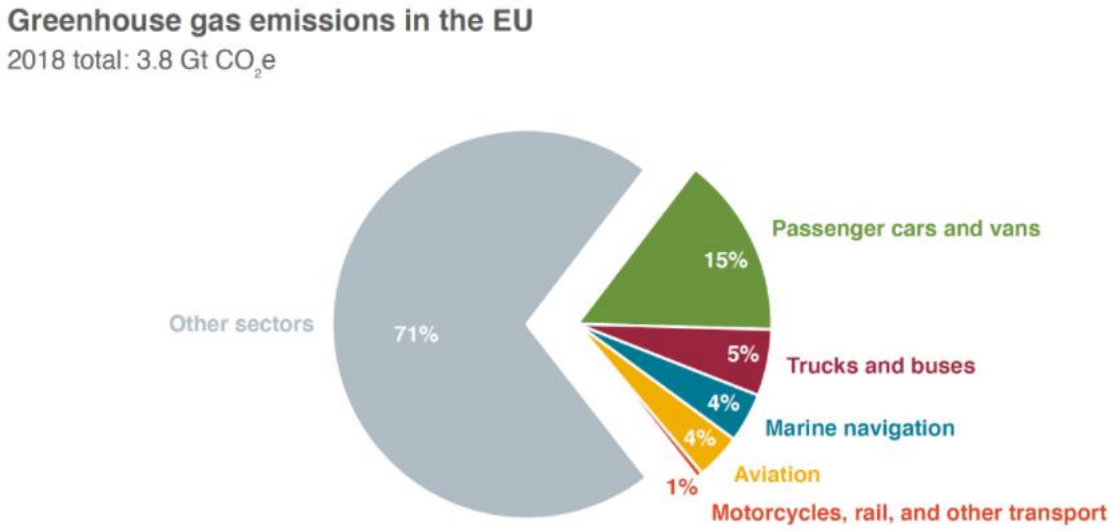

Figure 1: *Greenhouse gas emissions in the EU represented as transport sector percentage. (The International Council on Transport, 2021)*

While HDVs account for only 2% of all vehicles on the road in Europe, they are responsible for 27% of CO_2 emissions from road transport in the EU. (Transport & Enviroment, 2022) In concrete, heavy-duty trucks were responsible of 1776 Mt CO_2/year globally, more than double of the shipping or aviation emissions. (IEA, Tracking Transport, 2021) It is responsible for around 6.5% of worldwide CO_2 emissions. When compared to the light-duty sector, this industry does not reduce emissions. Their emissions are rapidly rising (increasing 9% from 2014 to 2019). Trucks, which are increasingly needed to deliver a variety of goods, are both useful and destructive to the environment (Transport & Enviroment, 2022).

The European Green Deal appeals to reach net-zero economy wide emissions and a 90% reduction in transport emissions by 2050. An analysis done by ICCT (Claire Buysse, 2021) evaluates tailpipe CO_2 emissions from light and heavy-duty vehicles in the EU from 2020 to 2050 under adopted policies and is compared with other three new scenarios: lower, moderate, and higher ambition. For HDVs, emissions evolve relatively flat, reducing only 19% of emissions in 2050 compared to 2020, while high ambition aims at the expected 90% reduction (*Figure 2*).

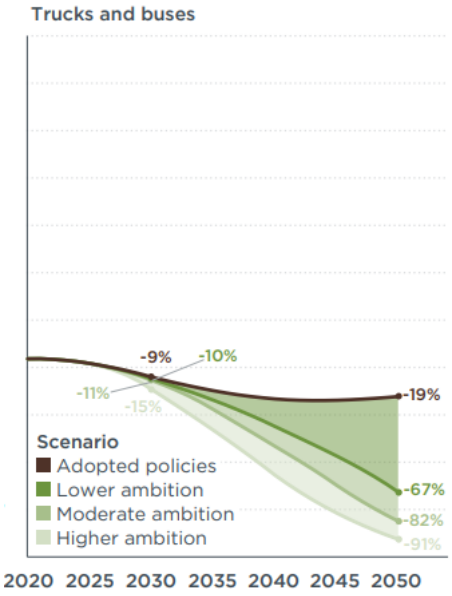

Figure 2: *CO2 Emissions reduction scenario (Claire Buysse, 2021).*

From 2025 on, truck manufacturers will have to meet the targets set for the fleet-wide average CO_2 emissions of their new lorries registered in a given calendar year. Stricter targets will start applying from 2030 on. The targets are expressed as a percentage reduction of emissions compared to EU average in the reference period (1 July 2019–30 June 2020):

- From 2025 onwards: 15%
- From 2030 onwards: 30%

The 2025 target can be achieved using technologies that are already available on the market. The 2030 target will be assessed in 2022 as part of the review of the regulation. As a first step, the CO_2 emission standards will cover large lorries, which account for 65% to 70% of all CO_2 emissions from heavy-duty vehicles. As part of the 2022 review, the Commission should assess the extension of the scope to other vehicle types such as smaller lorries, buses, coaches, and trailers. (H2Accelerate, 2021)

There are two technologies that stand out above the rest to decarbonise the heavy-duty sector: FCV and BE. It should be noted that BEV technology has a clear advantage over FCV technology as it has developed at a rapid pace in recent years in the automotive sector and price scalability is considerably better than FCV prices. Still, the latter has a long way to go and that is why this work focuses on this technology to compare its competence with already developed BEVs.

This paper does not want to be taken as an endorsement that FCV technology is better than BEV technology, it has to be clear that these two technologies must be complementary in order not to have a single path to decarbonisation of the sector and thus reach the targets sooner.

For heavy-duty trucks, slow refuelling and shorter operation ranges have an important impact on both cost of transport and logistics operations. This leads to the need to find a zero-emission option that can replace the traditional diesel alternative internal combustion truck without these drawbacks. An

option that allows the transport of high loads, fast refuelling, and a wide operating range. These characteristics are provided by FC technology. This technology applied to heavy-duty vehicles operates very similar to diesel trucks through fast refuelling times, similar ranges, and potentially lower total cost of ownership compared with BET with fast charging. (H2Accelerate, 2021)

FCVs have the potential to be full-service trucks, combining the advantages of zero-emission electric trucks with the capabilities of traditional diesel trucks. A FC truck's range could be comparable to that of a typical diesel-powered vehicle. This is a game-changer for the freight industry: there is now a zero-emission option that can handle routes that diesel fleets can. FC technology, as opposed to batteries can offer higher range even over difficult terrains. Because hydrogen fuel tanks have higher specific energy than batteries, FC vehicles can transport more cargo. A FC truck can be refuelled in five to fifteen minutes, allowing the fleet operator to keep the truck on the road longer, thus increasing profit. Charging batteries can pull commercial vehicles off the road for hours at a time, wasting time and money. (BALLARD, 2021)

1.2. Theoretical foundations

In order to develop this work, it is necessary to review the basic concepts that underpin the FC technology. To do this, it is necessary to start by explaining how a FC works.

1.2.1. FC Basics

A FC is an electrochemical energy converter that converts fuel's chemical energy into direct current (DC) power. Its operation is based on the following electrochemical reactions happening simultaneously on the anode and the cathode.

At the anode:

$$H_2 \rightarrow 2H^+ + 2e^- \qquad \textit{(Eq. 1)}$$

At the cathode:

$$^1/_2\, O_2 + 2H^+ + 2e^- \rightarrow H_2O \qquad \textit{(Eq. 2)}$$

Typically, a process for generating electricity from fuel entails several energy conversions steps: combustion of fuel to convert chemical energy into heat, steam generation, and then operation of a turbine to convert thermal energy into mechanical energy, which is then used to operate an electricity generator. The FC technology combines all these steps into a single unit with no moving parts. The

simplicity of the design draws a lot of attention. A FC is comparable to a battery in certain ways. It has an electrolyte as well as negative and positive electrodes, and it uses electrochemical reactions to generate DC electrical power. A FC, unlike a battery, requires a continuous supply of fuel and oxidant. The electrode of a FC, unlike those in a battery, do not undergo chemical changes.

FCFCs can be grouped by the type of electrolyte they use: Alkaline FCs (AFCs), Proton Exchange Membrane FCs (PEMFCs), Phosphoric acid FCs (PAFCs), Molten carbonate FCs (MCFCs) and Solid oxide FCs (SOFCs). PEM FCFC technology is considered to most suitable for transportation sector and portable energy frameworks due to its high specific power and high-dynamic capabilities and that is why this study is focused on this (Barbir, 2013).

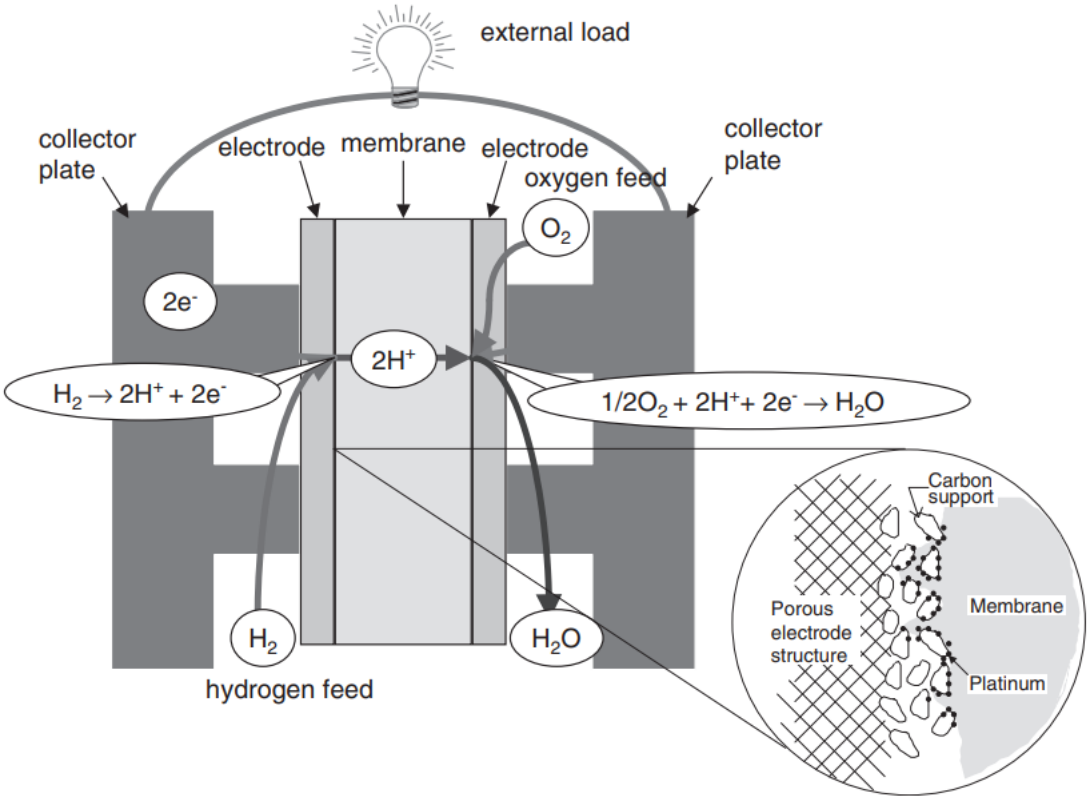

Figure 3: *Operation of a PEM FC. (Barbir, 2013)*

How does a PEM FC work? A polymer membrane, which has some special properties, is at the heart of a PEM FC. It is impermeable to gases, yet it conducts protons (hence the name proton exchange membrane). Between the two porous, electrically conducting electrodes, the electrolyte membrane is squeezed. Carbon cloth or carbon fibres paper are commonly used as gas diffusion layers. A layer of catalyst particles, commonly platinum supported on carbon, sits at the interface between the porous electrode and the polymer membrane. At the contact between the electrolyte and the membrane, electrochemical processes take place on the surface of the catalyst. Hydrogen, which is fed on one side of the membrane, separates into protons and electrons, which are its basic constituents. (*Figure 3*) Two electrons and two protons make up each hydrogen molecule. Electrons move through the outside circuit, while protons travel through the membrane. Electrons travel through electrically conductive electrodes, current collectors, and the outside circuit, thus producing a current and electrical work before returning to the opposite side of the membrane. The protons that passed through the

membrane and oxygen that is fed on that side of the membrane meet at the catalyst sites between the membrane and the other electrode. The electrochemical process produces water, which is then driven out of the cell by an excess of oxygen. The cumulative outcome of these simultaneous reactions is an electron current flowing through a direct electrical current circuit. The hydrogen side of the FCFC is negative and is referred to as the anode, whereas the oxygen side is positive and is referred to as the cathode (Barbir, 2013).

The electrolyte in the PEMFC is a thin (<50 mm) proton conducting polymer membrane (such as perfluoro sulfonated acid polymer). The catalyst is usually platinum supported on carbon with loadings of around 0.3 mg/cm^2, or Pt-Ru alloys are employed if the hydrogen supply contains minute amounts of CO. The operating temperature is usually between 60 and 80 ºC. PEM FCs are viable options for automotive applications, as well as small-scale distributed stationary power generation and portable electricity (Barbir, 2013).

Principal properties that characterise the FC:

1. High efficiency. As FC efficiency is higher than internal combustion engines, ranging from 45 to 60% at system level.
2. Zero tailpipe emissions. FCs operating on hydrogen generate zero emissions; the only exhaust is unused air and water. If methanol is used instead of hydrogen, some emissions are generated, including carbon dioxide. In general, these emissions are lower than those of comparable conventional energy conversion technologies.
3. No moving parts and potentially long life with adequate control strategy, as studied in this work.
4. Modularity. More power may be generated simply by adding more cells.
5. Low noise.
6. Size and weight. The size and weight of automotive FCs approaches those of internal combustion engines, and the size and weight of small FCs may offer advantage over the competing technologies.

1.2.2. Chemical & Thermodynamics

A basic chemical and thermodynamic foundation must be established to properly understand the physics behind FC technology. An amount of energy is released in an exothermic process that corresponds to the difference between the heat of the products and reactants. This is referred to as the reaction's heating value. When the reaction occurs at 25°C and atmospheric pressure, its value is measured as a greater heating value. The result of hydrogen combustion at these conditions is liquid water, however many processes produce gaseous water. A lower heating value is established as the difference between the higher value and the evaporation heat to account the water evaporation heat.

This is significant because the lower hydrogen heating value is utilized to calculate the system's energy input, mainly to compare FCs against other technologies such as internal combustion engines. It is the reference value against which the FC efficiency is tested, and it indicates the maximum amount of energy that might be taken from the fuel. The maximal energy output that can be transformed into

electricity is reduced by the entropy produced during the electrochemical reaction. The Gibbs free energy (ΔG) corresponds to this:

$$\Delta G = \Delta H - T\Delta S \quad \textit{(Eq. 3)}$$

The Gibbs free energy has a pressure dependency, which might impair the FC's operation. The Nernst Equation for hydrogen oxidation demonstrates this relationship.

$$\Delta G = \Delta G_0 + RT \ln \frac{P_{H_2O}}{P_{H_2} P_{O_2}^{0.5}} \quad \textit{(Eq. 4)}$$

Keeping this in mind, the theoretical potential of an FC, when combined with the current, represents the greatest amount of electrical power that could be extracted from hydrogen in an electrochemical process.

$$E = \frac{-\Delta G}{n \cdot F} \quad \textit{(Eq. 5)}$$

$$E = E_0 + \frac{R \cdot T}{n \cdot F} \cdot \ln\left(\frac{P_{H_2} \cdot P_{O_2}^{0.5}}{P_{H_2O}}\right) \quad \textit{(Eq. 6)}$$

Where F is the Faraday constant of 96.485 coulombs/electron-mol $\left(A\frac{s}{mol}\right)$, n is the number of electrons per molecule of H_2, R is the gas constant, and P and T are the pressure and temperature of each component. At 25°C, a hydrogen-oxygen FC has a theoretical cell potential of 1.23 volts.

The theoretical FC efficiency could be represented as the useable energy extracted from the total energy that can be obtained from hydrogen using this set. The theoretical FC efficiency would be 83 % if all Gibbs free energy could be converted into useable energy.

$$\eta = \frac{\Delta G}{\Delta H} \quad \textit{(Eq. 7)}$$

The lower heating value of hydrogen is frequently utilized to make a better comparison with an internal combustion engine, and since the process produces gaseous water as a product. This would result in a theoretical efficiency of 94.5 % or higher. Despite these encouraging figures, the theoretical FC efficiency and the Carnot Efficiency are analogous. The theoretical efficiency would generate no current, leaving it worthless, just as this efficiency is the greatest for a heat engine but would deliver no power. It is vital to consider the following areas to gain a deeper understanding of the actual FC's efficiency.

The rate of consumption of the reactants is proportional to the electric current density (i) and the charge transferred $(n \cdot F)$ (Eq.6). In the following points, a direct relationship between current density and reactant consumption will be used.

$$\dot{n}_x = \frac{I \cdot N_x}{n_x \cdot F} \qquad \textit{(Eq. 8)}$$

Where N denotes the number of single cells, I describes de current and n_x denotes the number of electrons exchanged per molecule of reactant, two in the case of hydrogen oxidation and four in the case of oxygen reduction. The consumption rate can also be calculated by multiplying the forward or backwards reaction rate coefficient (k_f or k_b) by the surface concentration of reactant species (C_{Ox} in the case of oxidation and C_{R_d} in the case of reduction). As a result, Equation 9 would be the electric current.

$$I = n \cdot F \cdot \left(k_f \cdot C_{Ox} - k_b \cdot C_{Rd}\right) \qquad \textit{(Eq. 9)}$$

The stoichiometry (λ) is the ratio of reactant excess in an electrochemical process. To avoid failures in the FC owing to design or water management concerns, the stoichiometry must always be greater than one, implying that there will be an excess of hydrogen injected into the FC that will not be used, and so will be lost if not recirculated. If hydrogen active recirculation is used in an FC system, a pump will be used to restore the pressure lost owing to pressure losses across the FC anode, as well as a filter to purify hydrogen if necessary.

1.2.3. Polarization Curve & Potential Losses

The voltage dependence on current density is expressed by the polarization curve, which is representative of an FC's performance. It's probably one of the most significant curves for describing FC behaviour and electrochemical losses. It is governed by electrochemical kinetics, which begins as soon as the circuit is closed and electrons and ions begin to move, supplying electric power but also voltage losses. In this way, activation polarization, internal currents and crossover losses, resistive losses, and concentration polarization can all be distinguished as voltage losses.

The voltage difference from equilibrium required to initiate an electrochemical reaction is known as activation polarization. It's linked to the slow electrode kinetics that show up at the start of the reaction. The Butler-Volmer equation describes the relationship between current density and activation losses, which is defined as the difference between the electrode potential (E) and the equilibrium potential (E_r), also known as overpotential.

$$i = i_0 \left(exp\left(\frac{-\alpha_{Rd} \cdot F \cdot (E - E_r)}{R \cdot T} \right) - exp\left(\frac{\alpha_{Ox} \cdot F \cdot (E - E_r)}{R \cdot T} \right) \right) \quad \textit{(Eq. 10)}$$

Where α_{Rd} and α_{Ox} are the transfer coefficients, and their values are frequently close to unity. By definition, the anode's equilibrium potential is 0 V, while the cathode's is 1.229 V.

The exchange current density (i_0), as described in the book (Barbir, 2013), is a way to evaluate an electrode's readiness to begin the electrochemical reaction before approaching the voltage losses in an FC. The smaller the energy barrier that the charge must overcome to activate the reaction and electrochemical processes, the higher the exchange current density.

The lower the exchange current density, the lower the activation polarization losses, because the energy required to initiate the reaction is lower, and the reaction will begin at lower current densities. Despite the fact that the overall reaction occurs in both electrodes, the cathode demands significantly larger overpotentials, resulting in a much slower reaction and dominating this loss process. The second term of the equation can be ignored for high negative overpotentials, allowing the Butler-Volmer equation to be stated more comprehensively.

$$\Delta V_{act,c} = E_{r,c} - E_c = \frac{R \cdot T}{\alpha_c \cdot F} \ln\left(\frac{i}{i_{0,c}} \right) \quad \textit{(Eq. 11)}$$

For positive overpotentials with the first term, a similar effect occurs at the anode, resulting in the equation:

$$\Delta V_{act,a} = E_a - E_{r,a} = \frac{R \cdot T}{\alpha_a \cdot F} \ln\left(\frac{i}{i_{0,a}} \right) \quad \textit{(Eq. 12)}$$

Because the activation potential loss in the anode is overshadowed by that in the cathode, the effect of activation polarization on the FCs potential will be as described in Equation 12.

$$E_{cell} = E_r - \frac{R \cdot T}{\alpha \cdot F} \ln\left(\frac{i}{i_0} \right) \quad \textit{(Eq. 13)}$$

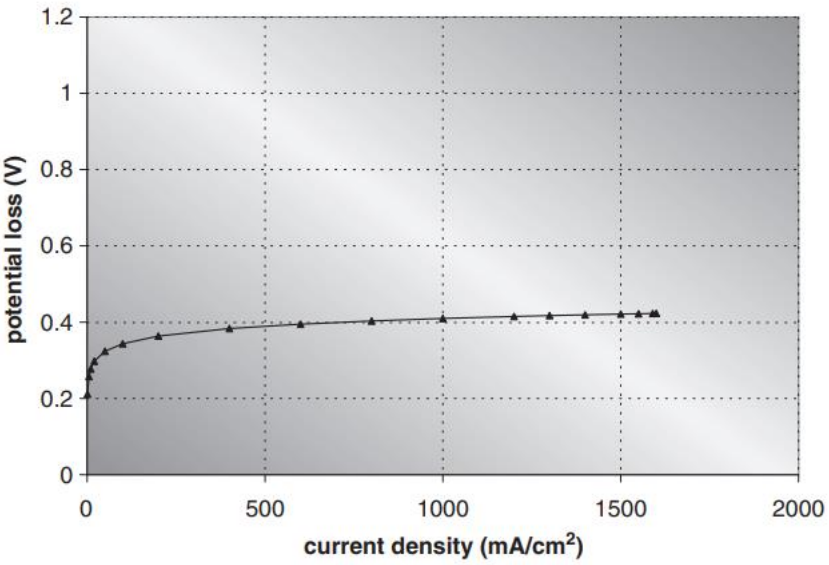

Figure 4: *Potential loss due to activation polarization only. (Barbir, 2013)*

Figure 4 shows that these potential losses increase more at low current densities but stay higher over a wide range of current densities. As a result, at low current densities, one source of potential loss will take precedence over the other losses.

Another reason for the drop-offs is that some hydrogen may diffuse from one electrode to the next, and some electrons will take a "shortcut" across the polymer membrane rather than sweeping down the external circuit. Crossover and internal current losses are terms used to describe this. They both have a comparable effect on voltage losses because each molecule of hydrogen that diffuses through the electrolyte and carries two electrons with it reduces the number of electrons contributing to the electrical current by two. The effect of the fuel crossover is minor in comparison to the rate of fuel and oxygen consumption, but these losses are substantial in an open circuit or at very low current densities.

The higher the internal current, the lower the cell potential, as seen in figure. As the difference in cell potential with internal losses grows, this has a greater effect as the current density decreases.

The hydrogen crossover is determined by the permeability, thickness, and partial pressure of hydrogen, which is proportional to hydrogen concentration at the catalyst surface. When the FC begins to generate electric current, the hydrogen concentration drops as it uses energy, reducing diffusion through the membrane.

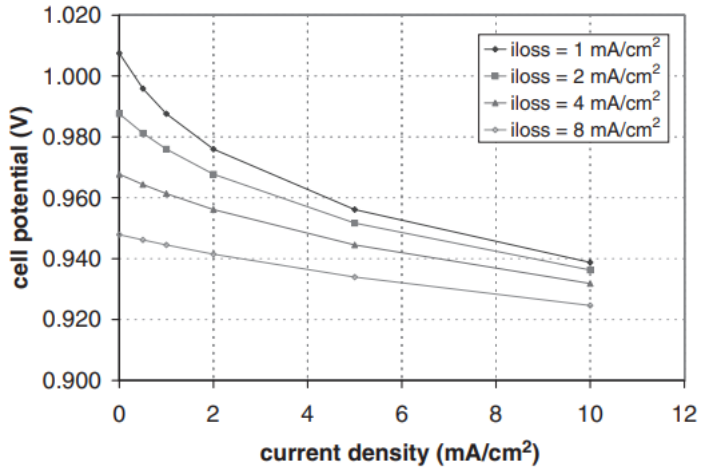

Figure 5: *Hydrogen crossover & internal current losses on an open circuit potential. (Barbir, 2013)*

The ohmic or resistive losses are a third voltage loss that has a significant impact on the FC performance. These are the losses caused by ion flow in the electrolyte and electron movement via the cell's conductive components (electrodes, circuits, connectors, etc.). It is the most basic loss mechanism because it is based solely on Ohm's law. As demonstrated in *figure 6*, they have a bigger impact at medium to high current densities, dominating potential losses in this range.

$$E_{ohm} = i \cdot R_i \qquad \textit{(Eq. 14)}$$

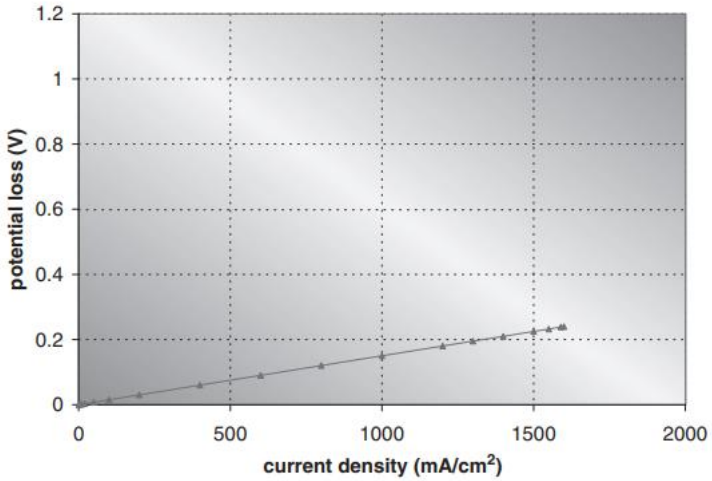

Figure 6: *Potential losses due to ohmic losses only. (Barbir, 2013)*

Concentration polarization is a final source of possible losses that has a significant impact on the efficiency of the FCs. When a reactant is rapidly consumed at the electrode at a rate faster than the reactant supply rate, which is restricted by the electrode's material properties, a concentration gradient appears. The reaction potential is determined by the partial pressures of the reactants, which are influenced by the concentration of each species, as stated in Equation 6, which is derived from the Nernst Equation.

$$p_x = C_x \cdot R \cdot T \qquad \textit{(Eq. 15)}$$

The Fick's law expresses the relationship between the flow of reactants and the concentration gradients on a one-dimensional diffusion, which can also link to the electrical current produced, for a better understanding.

$$N = \frac{D \cdot (C_B - C_S)}{\delta} \cdot A = \frac{I}{n \cdot F} \qquad \textit{(Eq. 16)}$$

D is the reacting species' diffusion coefficient, A is the electrode active area, δ is the diffusion distance that the reactants must traverse, and C_B and C_S are the reactant's bulk and surface concentrations, respectively.

The current density can be calculated as a function of concentration using this set.

$$i = \frac{I}{A} = \frac{n \cdot F \cdot (C_B - C_S)}{\delta} \qquad \textit{(Eq. 17)}$$

Because the concentration at the catalyst's surface is dependent on the current density, the relationship can be established in both directions. As a result, the concentration gradient will be higher the higher the current density. When the reactant is consumed at the same rate as it is supplied, the surface concentration reaches zero. The limiting current density (i_L) is the current density at which this occurs, and it limits the maximum current that may be expected from the FC.

As a result, at this limiting current density, the potential losses owing to concentration polarization would be characterized as shown in Equation 18.

However, this would result in a sharp decrease in the cell's potential, which contradicts empirical findings, which show a more gradual increase in potential losses. The *figure 7* demonstrate this.

$$\Delta V_{conc} = \frac{R \cdot T}{n \cdot F} \cdot \ln\left(\frac{i_L}{i_L - i}\right) \qquad \textit{(Eq. 18)}$$

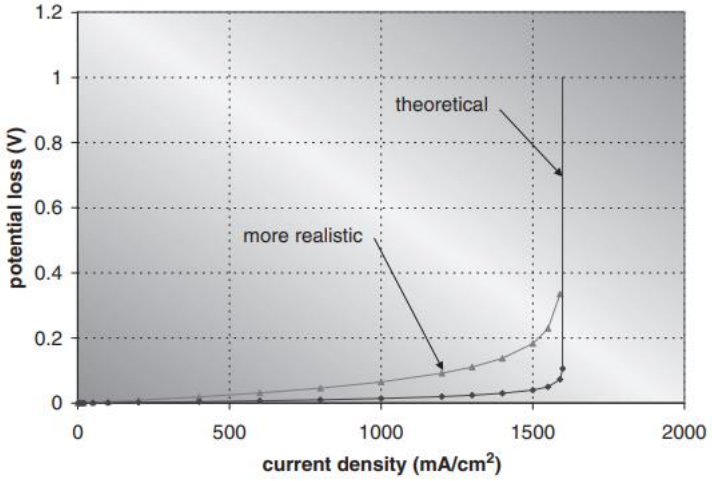

Figure 7: *Potential losses due to concentration losses. (Barbir, 2013)*

Now it's time to define the polarization curve accurately and discuss its significance. It explains how the FC potential and current density are related. It is unique to each FC and can be used to explain the electrochemical device's overall operation. It is possible to establish a management strategy that will maintain the system functioning at the current density required while assuring maximum efficiency by recognizing the polarization curve of an FC. It also represents the cell's limitations, which aids in determining whether the equipment can perform the task.

As a result, the potential losses at each current density alter this curve. When each loss is compared, the activation is clearly superior, implying that it dominates the FC's overall performance in terms of voltage losses. The FC potential, on the other hand, is influenced by a combination of them, each of which has a different effect at different current densities and illustrates how the FC potential changes from the theoretical and equilibrium potential as the current density rises.

$$E_{cell} = E_{r,T,P} - \frac{R \cdot T}{\alpha \cdot F} \cdot \ln\left(\frac{i}{i_0}\right) - C \cdot \ln\left(\frac{i_L}{i_L - i}\right) - i \cdot R_i \qquad \textit{(Eq. 19)}$$

Where C is a loss per concentration coefficient which refers to $\frac{R \cdot T}{n \cdot F}$.

The *figure 8* accurately depicts the total effect of each voltage loss and aids in seeing the relative relevance of each at various current densities. These will influence the operation regimens that the FC must follow to achieve maximum efficiency.

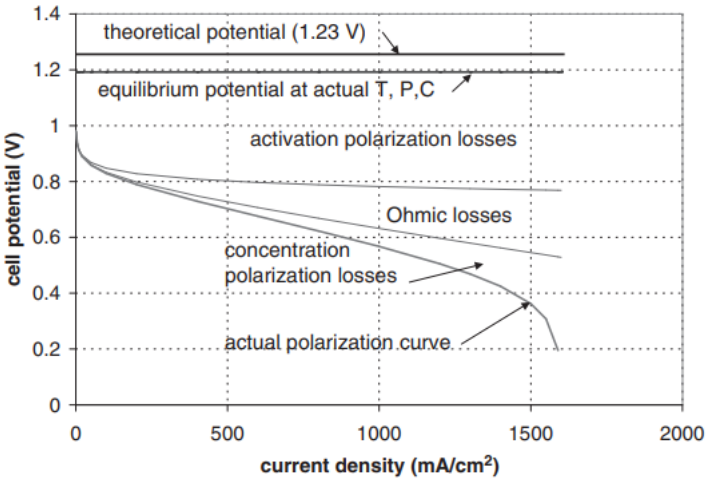

Figure 8: *Polarization curve and the effect of each voltage loss. (Barbir, 2013)*

The polarization curve and potential losses are inextricably linked to the electrical power that an FC can generate. In fact, the electric power generated is equal to the FC's potential multiplied by the electrical current, both of which are related through the polarization curve.

As a result, the losses above stated will have an impact on power generation and, as a result, the FC's efficiency. This is the ratio of the electric gross power (P_{el}) of the stack to the chemical power of the consumed hydrogen $\left(P_{H_2}\right)$, with the higher heating value times the hydrogen consumption rate.

$$\eta = \frac{P_{el}}{P_{H_2}} = \frac{I \cdot V}{\Delta H \cdot N_{H_2}} \qquad \textit{(Eq. 20)}$$

Where ΔH is the lower heating value of hydrogen in $\frac{J}{mol}$ and N_{H_2} is the rate of fuel consumption in $\frac{mol}{s}$. This can be improved to express efficiency as a percentage of voltages. The energy resulting from hydrogen consumption can be expressed in this way, thanks to Faraday's law:

$$P_{H_2} = \Delta H \cdot \frac{I}{n \cdot F} \qquad \textit{(Eq. 21)}$$

This has voltage unities, resulting in 1.482 V for the higher heating value and 1.254 V for the lower heating value when utilizing the higher heating value. Now it's time to think about the losses discussed before, because they'll change not just the voltage and electrical power, but also the hydrogen effective consumption in the case of hydrogen diffusion, internal currents, or excess hydrogen injected into the system. As a result, the efficiency of the FC can be expressed as a product of prospective efficiency times present efficiency.

$$\eta = \frac{V}{1.254} \cdot \frac{i}{(i + i_{loss})} \qquad \textit{(Eq. 22)}$$

The polarization curve can be linked to other parameters besides efficiency. Power density is defined as the power per unit of area, which is calculated by multiplying the voltage by the current density. A maximum in power density can be seen by graphing both values together (*figure 9*), indicating that there is no need to operate an FC any further.

Because the cell potential and efficiency are directly related, the greatest power density would be achieved at a significantly lower efficiency than the optimum. This is extremely significant information since, for a given power demand, a larger FC would result in a lower power density and higher efficiency, whereas a smaller FC would result in the opposite: a higher power density but at the expense of efficiency loss.

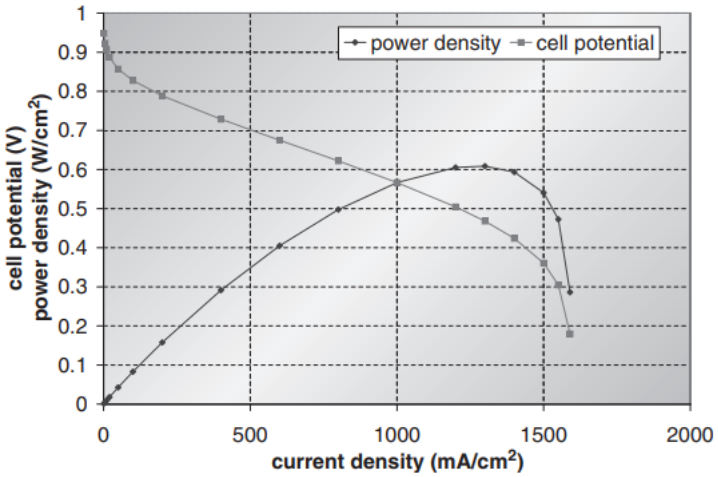

Figure 9: *Polarization and power density curves. (Barbir, 2013)*

1.2.4. Hydrogen as a fuel

Hydrogen is a clean fuel that produces just water when consumed in a FCFC. Hydrogen can be made from a range of domestic sources, including natural gas, nuclear power, biomass, and renewable energy sources such as solar and wind power. These characteristics make it a desirable fuel for transportation and electricity generation. It can be utilized in automobiles, homes, portable power, and a variety of other applications. Hydrogen is an energy carrier that may be utilized to store, transport, and deliver energy generated by other sources. (ENERGY.GOV, s.f.)

Today, hydrogen fuel can be produced through several methods:

1. Steam reforming: a high-temperature process in which steam combines with a hydrocarbon fuel to produce hydrogen, is a common thermal technique for hydrogen production. Natural gas, diesel, renewable liquid fuels, gasified coal, and gasified biomass are just a few of the hydrocarbon fuels that can be reformed to produce hydrogen. Today, natural gas steam reforming produces around 95% of all hydrogen.
2. Electrolysis is a technique for separating water into oxygen and hydrogen. Electrolytic activities are carried out in an electrolyser, which works similarly to a FC but in reverse: instead of harnessing the energy of a hydrogen molecule, an electrolyser generates hydrogen from water molecules.
3. Light is used as a catalyst in solar-powered hydrogen synthesis. Photo-biological, photoelectrochemical, and solar thermochemical processes are only a few of the solar-driven processes. To manufacture hydrogen, photo-biological systems rely on the natural photosynthetic activity of bacteria and green algae. Photoelectrochemical techniques split water into hydrogen and oxygen using specific semiconductors. Sun thermochemical hydrogen production uses concentrated solar energy to drive water splitting processes, which frequently include additional species like metal oxides.
4. Microbes such as bacteria and microalgae are used in biological processes, which can produce hydrogen through biological reactions. Microbes break down organic matter such as biomass or wastewater to produce hydrogen in microbial biomass conversion, whereas photo-biological processes use sunlight as an energy source. (ENERGY.GOV, s.f.)

Hydrogen (H_2) is attracting unprecedented interest and investment, owing to a global shift in regulators, investors, and consumers toward decarbonization. Over 30 nations have established hydrogen roadmaps, the industry has declared more than 200 hydrogen projects and aggressive investment plans, and governments around the world have pledged more than USD 70 billion in public funding as of the beginning of 2021. This momentum is boosting cost reductions for hydrogen production, transmission, distribution, retail, and end uses across the whole value chain. (Company, 2021)

Given the wide spectrum of H_2 manufacturing processes, H_2 has a higher energy density than batteries in the transportation sector, enabling long-range displacements (>500 km) and lower cradle-to-grave emissions than hydrocarbon-fuelled cars (Novella, 2020). Furthermore, FC systems are easier to scale than batteries since they have a lower specific power and power density. As a result, H_2 is the only alternative for decarbonizing the operation of heavy-duty vehicles, ships, trains, and aircraft, while it is a perfect complement and coexisting fuel for light-duty vehicles, enabling long-range, carbon-free passenger cars (Undertaking, 2019) (Agency, 2019)

1.2.5. FC vehicles: non-plug-in FCV and FCREx

Many factors can be used to classify FC vehicles, including the fuel storage technique (pressurized H_2 or liquid carriers that must be reformed/cracked), the power system topology (direct or indirect), and the battery charging capability (plug-in or non-plug-in). The Honda Clarity, Hyundai Nexo, and Toyota

Mirai commercial FCVs now use an indirect-type power design with H_2 stored at 700 bar of pressure and small-capacity batteries (non-plug-in). It is acceptable to use the indirect type of power architecture to lower the size of the FC system and compressed H_2 because this technology has been reliably shown (high TRL) (Teng T, 2020) in terms of the power system structure and fuel storage of these cars. Despite the lack of light-duty plug-in vehicles on the market, they should not be discarded because they can provide considerable advantages over non-plug-in vehicles. Lower degradation rates, potentially improved performance, increased operational flexibility, and potentially lower TCO and cradle-to-grave emissions are just a few of the advantages. (Novella, 2021)

Because both the FC and the battery may minimize power and battery state-of-charge (SoC) variations, plug-in FCVs use the FC as a range extender (FCREx). The FC stack is subjected to power fluctuations in non-plug-in vehicles, as well as frequent start and stop, which causes deterioration, resulting in a drop in performance and an increase in user costs. In-depth battery drain or a high SoC, on the other hand, reduces battery durability and performance. As a result, maintaining a battery's SoC at a modest and consistent level extends its life and lowers user maintenance expenses.

Recent technological studies of commercial FCVs have revealed that current-generation FC systems can exhibit extremely dynamic behaviour, sufficient to meet the power demands of aggressive driving cycles with small batteries. As a result, the reliable operation of FCREx may also help to reduce H_2 usage.

The FCREx's larger batteries provide for more flexibility in operation, allowing for both pure electrical and hybrid modes, depending on the user's needs. This is especially significant given the current circumstances, since the cost of hydrogen is far higher than that of electricity, and there are few hydrogen refilling stations around the world as you can see below.

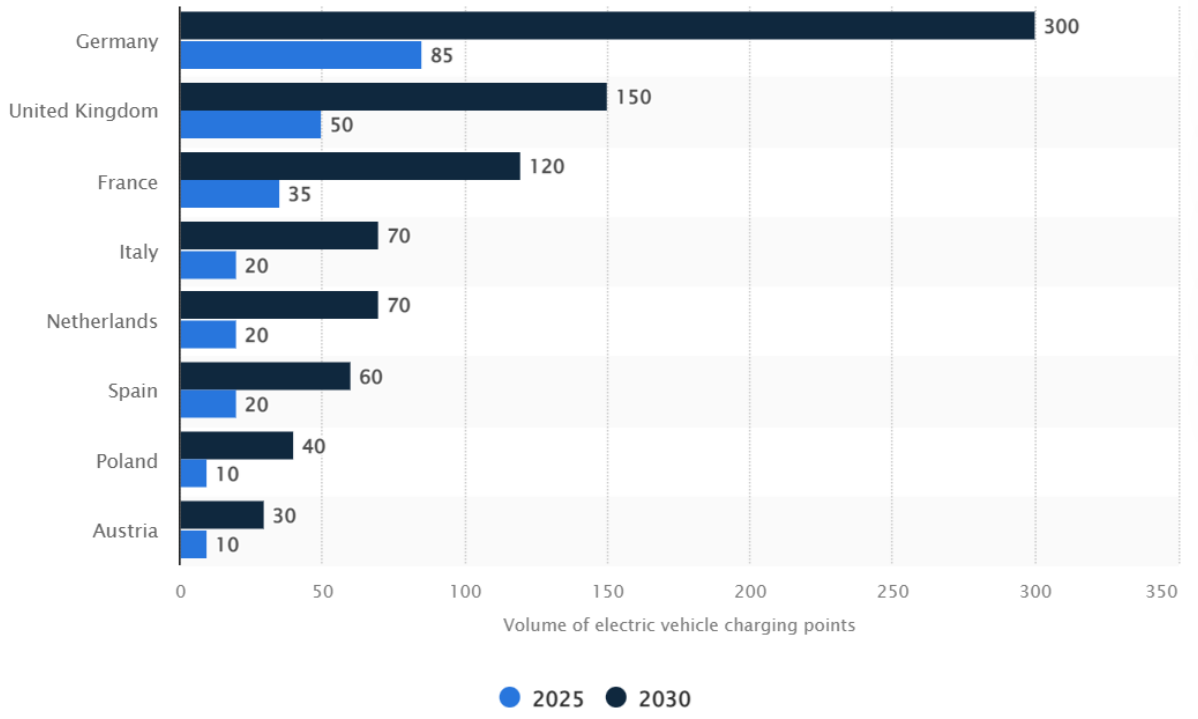

Figure 10: *Number of hydrogen refilling stations in Europe. (ACEA, 2021)*

Finally, if the battery is not over-dimensioned, the TCO for an FCREx may be reduced. The total cost of ownership (TCO) includes the vehicle's purchase price, insurance, fuel or energy source costs, maintenance, and numerous taxes and levies. Assuming that insurance and taxes/fees for FCREx and non-plug-in FCV are substantially the same, FCREx could lower the TCO for a variety of reasons. First, because the battery capacity is bigger, the maximum net power of the FC system can be reduced. As a result, the stack and all other components of the FC system should need less power and be less expensive. However, the increased expense of manufacturing a larger battery could overcome this. Second, because H_2 is currently more expensive than electricity when produced using the same electrical mix, the operating expenses of an FCV may be higher than those of a BEV. Using a combination of electricity and H_2 to lower the TCO of FCV is one possibility. (Novella, 2021)

2. OBJECTIVES

The aim of this final degree project is to optimize the performance and durability of a hydrogen multi-FC system for heavy duty transport. To achieve this objective, it has been necessary to carry out a series of parallel objectives:

- Simulate all the possible combinations of this multi-FC system with GT-Suite and MATLAB Simulink.
- Examine various FC-battery combinations.
- Analyse the best control strategies to reduce the system's hydrogen consumption.
- Determine the optimal FC combination in terms of FC durability.
- Calculate the Total Cost of Ownership and the Life Cycle Assessment of this technology and determine the optimal designs.

In a different sense, this initiative strives to extend knowledge on additional energy sources for the industry sector, beginning with hydrogen as a possible fuel, and acts as a foundation for future academic studies in this field, from the perspective of a final master's degree student. It will also explain the repercussions of these types of projects so that you may better understand what an engineer does. Finally, through using programs like GT-Suite and MATLAB Simulink, it is hoped to develop familiarity with simulation software tools in preparation for future use.

3. METHODOLOGY

The methodology followed to prepare this final master's degree project is illustrated in the following block diagram. As can be seen, research of various scientific articles related to this technology applied to heavy-duty transport has been done to identify the various knowledge gaps in the literature where it has not been investigated. Then, starting from the basis of the hydrogen FC range extender design provided in the article (Novella, 2021) and the research group's work on this technology applied to the passenger car model, a similar methodology has been followed but now applied to a heavy-duty transport application with a multiple FC system (more than one FC operating), specifically one with similar characteristics to the Hyundai Xcient FC. A validated FC model was used and integrated into a

scalable balance of plant to conform an FC system to perform the simulations required to analyse the effect of FC stack sizing and dynamic limitations on the performance and durability of FCREx vehicles. Previous studies optimized the management of the balance of plant component to maximize FC system efficiency. The model that resulted was integrated into an FCV architecture. To perform the WLTC 3b driving cycle simulations in fair conditions, energy management optimizer algorithms and semi-empirical semi-physical degradation models were developed and integrated in parallel. This section intends to cover all of the important aspects of the modelling procedure, but it focuses heavily on the development of the degradation model, as it is the main novelty in the methodology of this study. Previous studies performed and extensively explained the FC stack model, the management of the balance of plant architecture, and the design of the FCV architecture [7, 8].

The GT-Suite v2020 software was used to model the FCV. This numerical tool, which is a 0D-1D thermal fluid-dynamics modelling platform that solves the continuity, momentum, energy, and species equations numerically using well-known and widely accepted physically based correlations, is widely used in the automotive industry and for research reasons. The degradation model and the energy management plan optimizer were developed in MATLAB R2020a software and integrated to GT-Suite to perform the driving cycle simulations as a complement to this modelling tool.

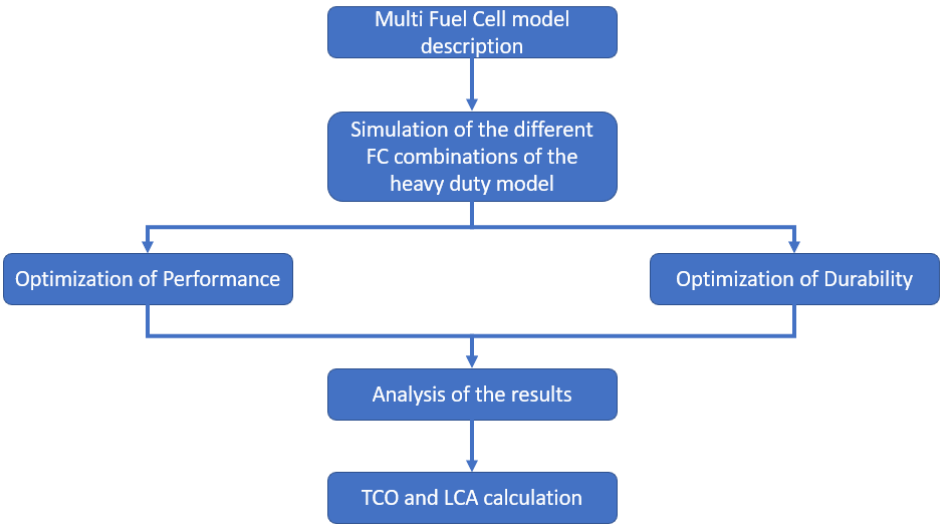

Figure 11: *Methodology diagram.*

3.1. Multi FC model description

3.1.1. FC model description

The polarization curve of the FC stack model used in this study is defined as follows:

$$V_{FC} = V_{OC} - V_{act} - V_{ohm} - V_{conc} \quad \textit{(Eq. 23)}$$

$$V_{OC} = \frac{-\Delta \overline{g_f}}{2F} \quad \textit{(Eq. 24)}$$

$$V_{act} = \begin{cases} \frac{R_{gas}T}{2F}\left(\frac{i}{i_0}\right) \\ \frac{R_{gas}T}{2F}\ln\left(\frac{i}{i_0}\right) \end{cases} \quad \textit{(Eq. 25)}$$

$$V_{ohm} = R \cdot I \quad \textit{(Eq. 26)}$$

$$V_{mt} = -C\ln\left(1 - \frac{i}{i_l}\right) \quad \textit{(Eq. 27)}$$

where V_{act}, V_{ohm}, and V_{conc} are the activation, ohmic, and mass transmission losses, and V_{OC} is the open voltage circuit. Advanced losses modelling was used to take into account how the ohmic resistance and exchange current density were affected by the FC operating conditions. Modelled variables were temperature, oxygen partial pressure, electrode roughness, and reference exchange current density dependency on exchange current density i_0. (Dominik Murschenhofer, 2018). Based on a reference ohmic resistance, ohmic resistance (R) was modelled by considering the change in membrane ionic resistance with membrane water content, as in (Kobunshi, 2008). Following the experimental data in (P. Corbo, 2007) (P. Corbo, 2008), the reference exchange current density, reference ohmic resistance, charge transfer coefficient, mass transport loss coefficient (C), limiting current density (i_l), and voltage open circuit losses values were calibrated to validate the model at different pressure and temperature conditions. The GT-Suite genetic algorithms toolkit was used to calibrate the model and keep the overall error between experimental and numerical results under 2%. (*figure 12*). Because the FC stack is anticipated to be subjected to varying operating conditions depending on the environment and the operation of the BoP components in driving cycle conditions, this study differs from previous ones in that the FC model was validated by comparing numerical to experimental polarization curves at various pressure and temperature conditions concurrently. The FC model was then integrated into a balance of plant model (*figure 13*) that had previously been created and optimized (Novella, 2021). A set of components for the anode, cathode, and cooling circuits make up the BoP. An active H_2 recirculation loop drives back the fuel excess to the stack with an H_2 pump that is also used to control anode stoichiometry. The active H_2 recirculation loop sends back the extra fuel to the stack using a H_2pump, which is also used to control the anode stoichiometry, and the H_2tank connected to the stack by a valve controls the anode pressure. The cathode circuit has an electric centrifugal compressor, a heat exchanger to chill the air, and a humidifier to increase the relative humidity of the air at the FC stack cathode inlet in order to reduce ohmic losses. The humidifier raises the water content of the air at the cathode inlet using the gases at the cathode exit, which are

primarily water vapour and air with low oxygen concentration. The cathode pressure is adjusted by varying the power supplied to the electric motor, whilst the air mass flow is controlled by modifying the throat area of a valve at the cathode circuit's outlet. The computations consider the consumption of each component, and PID controllers are employed to regulate them.

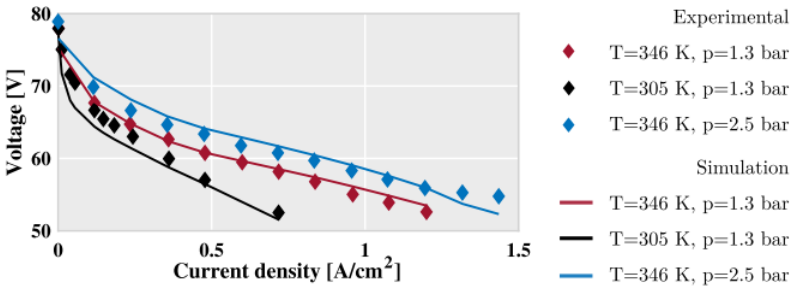

Figure 12: *Calibration of the FC stack model to experimental data under different pressure and temperature conditions measured at the cathode outlet. (Novella, 2021)*

3.1.2. Multi FC system

The system is split into two parts: the FC stack and the Balance of Plant (BoP). The FC stack is a collection of FCs in which the reaction occurs at the same time. The voltage and currents required to meet the application are provided by a combination of sufficient cells. The BoP is the sum of all auxiliary systems that contribute to the device's operation. It is organized into three subsystems or circuits: anode, cathode, and coolant. For each FC, the BoP architecture remains the same, but the components that make it up must be adapted to the FC stack. Because the BoP uses energy from the FC stack, as shown in *figure 13*, the system's net power and efficiency will be influenced by the actuation of each component.

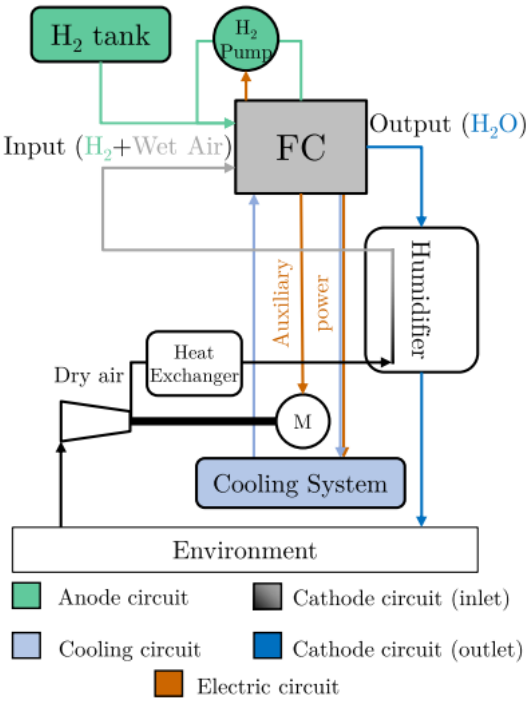

Figure 13: *FC system schematic integrating all the inner circuits. (Novella, 2021)*

The designs studied are scaled versions of the baseline architecture of the validated 20 kW PEMFC with its balance of plant or BoP. Our Multi FC system is composed by 2 FCs making up a total of 240 kW of power. The combinations studied throughout the paper are $80 + 160$, $120 + 120$ and $100 + 140kW$. The cathode side, anode side, and cooling side of the BoP architecture are as follows:

1. On the cathode side, an e-charger compressor supplied high-pressure air to the FC stack, a heat exchanger served as an intercooler, and a humidifier system used water from the FC stack exhaust to raise the cathode inlet relative humidity (RH):

- The pressure and air mass flow rate requirements of the FC stack were parametrized in the centrifugal compressor map (*figure 15*). This was required for sizing because the compressor specifications differed depending on the size of the FC stack. Two PIDs were used to manage cathode stoichiometry and pressure, the first acting on the power provided to the e-charger and the second acting on the exhaust valve area.

- The heat exchanger was designed with a continuous cooling efficiency of 70% and a coolant temperature of 70°C as the cold reservoir.

- To account for heat transfer, the humidifier system was modelled using 7000 pairs of 500 mm-long pipes joined by a thermal mass. Water ejectors and injectors were used to simulate water transfer. The humidifier was utilized to keep the cathode inlet RH at 80% to assure membrane humidification even when the load changed suddenly.

2. A 350 bar H_2 tank and an active H_2 recirculating loop were installed on the anode side (powered by a pump). The anode pressure was controlled by the pump, which was driven by the FC, and the anode stoichiometry was controlled by the valve between the recirculating loop to the H_2 tank.

3. The cooling system included a cooling pump that was powered by the FC and a radiator that kept the coolant temperature at 70 degrees Celsius. The cooling system in *figure 13* was simplified by not showing it in detail because it is not significantly different from those used in normal automobiles.

Because all systems that conform to the BoP demand power from the FC to run, the net power that may be gained from the system is conditional on the performance of each component. As a result, the net power (P_{Net}) is equal to the electrical power (P_{el}) collected from the FC stack (as voltage times current) minus the power dedicated to the compressor (P_{comp}), hydrogen pump ($P_{H_2\ pump}$), and coolant pump ($P_{cool\ pump}$). The net power divided by the fuel power spent would be the efficiency of the FC system, which truly reflects the performance of the devices (being the fuel consumed times it lower heat value).

$$P_{\ Net} = P_{el} - P_{comp} - P_{H_2\ pump} - P_{cool\ pump} \qquad \textit{(Eq. 28)}$$

$$\eta = \frac{P_{\ Net}}{LHV \cdot \dot{m}_{H_2}} \qquad \textit{(Eq. 29)}$$

In the same study as mentioned, it was necessary to optimize the operating conditions of the BoP as there are some parameters as stoichiometry, pressure, temperature and relative humidity at both anode and cathode that affect the performance of the FC stack. The cathode stoichiometry and pressure, in particular, have a significant impact on the FC system performance because their values are coupled with the compressor consumption, which is significantly higher than that of the H_2 recirculating pump or the coolant pump.

As such, in this study, the optimization of the BoP was performed by optimizing the air management strategy with the FC stack load to maximize the FC system efficiency. It was performed in steady-state conditions and for the baseline design. The stoichiometry and the cathode inlet pressure were varied in the range of 1.8 to 60 (the highest values correspond to extremely low load) and from 1.2 to 2.5 bar (to preserve mechanical integrity) respectively as shown in the *figure 14*.

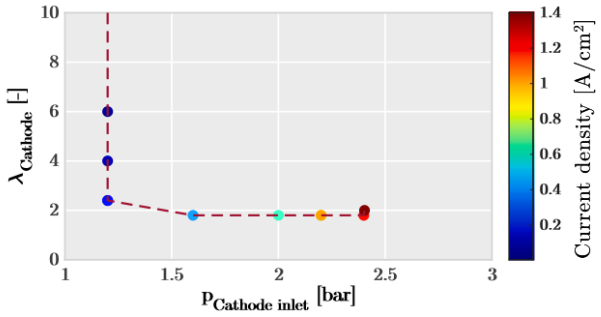

Figure 14: *Optimum cathode inlet pressure and stoichiometry at different current densities (load). (Novella, 2021)*

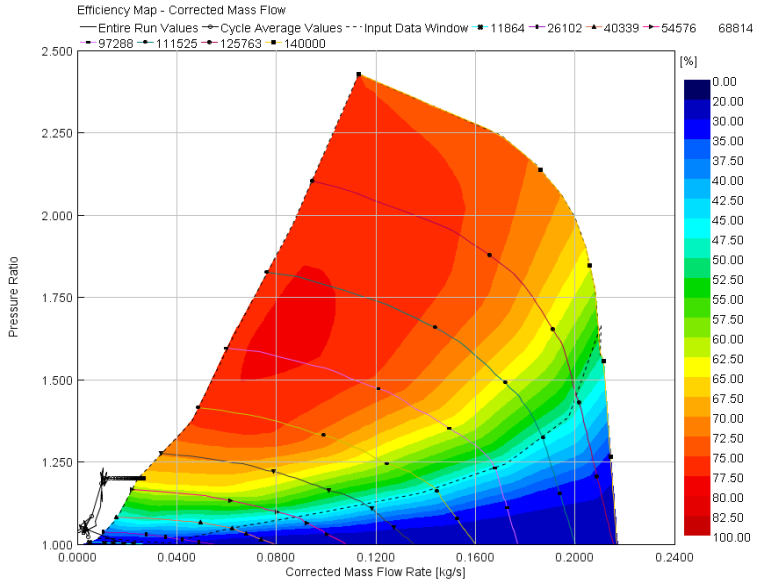

Figure 15: *Parametrized compressor map with optimum operating conditions.*

From *figure 15*, it can be deduced that the best air management strategy for an FC system, as in ICE, is to minimize compressor wasted energy, i.e., the best compressor pressure ratio for a given cathode stoichiometry (mass flow) is the one with the highest efficiency. This means that increasing the FC stack fuel efficiency with air pressure has a rather minor influence on the BoP operating conditions optimization. (Novella, 2021)

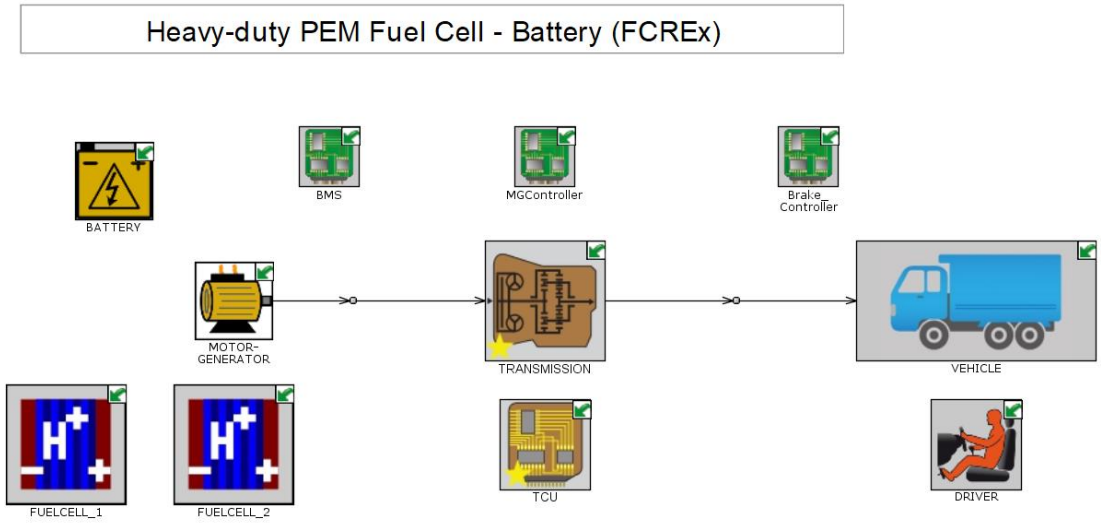

Figure 16*: GT-Suite block diagram picture of the heavy-duty PEM FC-battery system*

3.1.3. Battery

The high-voltage battery pack of the truck has 73.2 kWh of capacity. It is a Li-ion battery due to the energy density that offers compared to other batteries in the market. But this battery is scaled up from a base battery with the following features: This battery was designed as a series of 100 cylindrical cells to give enough power for the purely electric mode and n parallel of parallel cells to enforce the battery capacity. Each cylindrical cell had a nominal voltage of 3.6 V and a nominal capacity of 3.35 Ah, and it was modelled using an equivalent electric circuit (RC) whose open-circuit voltage and resistance were dependent on the state of charge and battery temperature. To ensure that the battery does not overheat, a lumped mass thermal model was applied. The influence of temperature on the battery, however, was not considered due to a lack of data. Finally, the battery's DC/DC converter and the electric motor's DC/AC converter were both modelled with a constant conversion efficiency of 95%.

3.1.4. Truck body

In this project, a vehicle body similar to the Hyundai Xcient FC was used. The empty vehicle weight is 9,795 kg with a max gross vehicle weight of 19,000 kg as rigid truck. The dimensions of the truck are those shown in the *figure 16* (in mm).

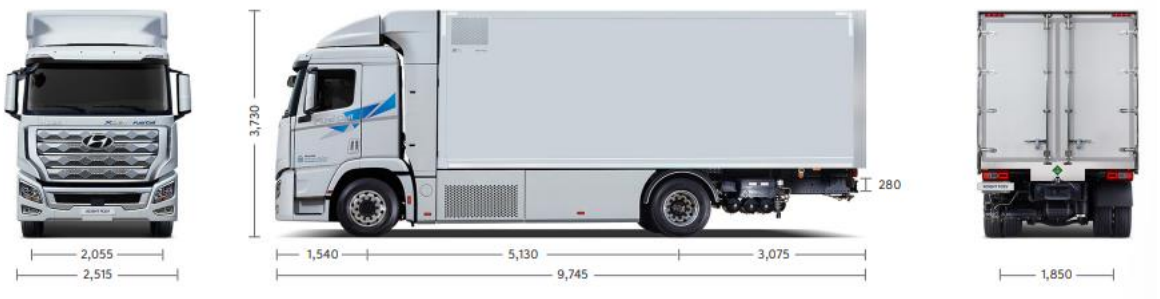

Figure 17: *Hyundai Xcient FC body measures. (Hyundai Truck and Bus, s.f.)*

It is a 4x2 rigid truck, with a hydrogen tank capacity of 32.09 kg distributed among 7 tanks. Based on commercial FC system data (BALLARD, Product Data Sheet - FCVelocity-MD, 2016) (BALLARD, Product Data Sheet - FCMove-HD, 2016), the vehicle mass was changed by considering the specific power of the FC system as a scaling factor.

It was decided that the vehicle's electrical architecture would be indirect (Novella, 2021). This approach, while potentially less efficient than the direct option, provides for increased FC lifetime due to protection from system bus electric fluctuations and downsizing of the FC system due to the DC/DC converter (Teng T, A comprehensive review of energy management optimization strategies for fuel cell passenger vehicle, 2020). To account for these power losses, the conversion efficiency of each DC/DC or DC/AC converter was assumed to be constant and equal to 95%.

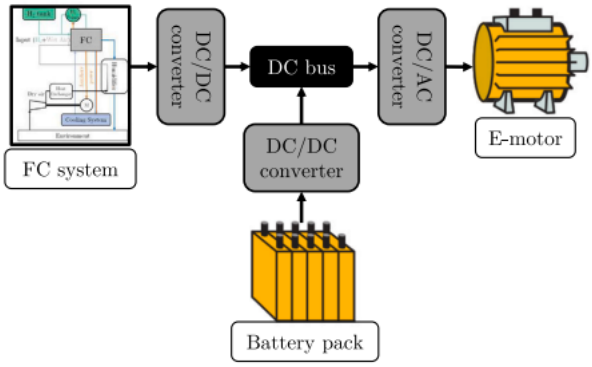

Figure 18: *Powerplant electronic configuration. (Novella, 2021)*

The shaft is driven by an electric motor with a maximum power of 350 kW and a torque–power curve that offers sufficient torque even at high loads. A direct drive connection was established between the e-motor and the shaft.

3.2. Energy management strategy (EMS)

In a powertrain with several energy sources, energy management fundamentally involves determining the best power split sequence that meets the design criteria at the lowest cost (Onori S, 2016). It is a critical feature that governs, to a large extent, the whole system's performance. In this regard, an ineffective power split technique may skew the benchmark between different sizing combinations, resulting in a skewed choice on which powertrain sizing is optimum. Optimal Control (OC) is a tool that is particularly well suited to developing an energy management strategy in a benchmark study like the one provided in this research, as it naturally gives the optimal energy split for each powertrain under consideration. As a result, all the architectures under consideration will be contrasted in the most favourable light. (Luján JM, 2016)

In keeping with the preceding concept, the OC problem, which entails determining the powertrain control strategy that minimizes a cost index across the driving cycle in question, it has been solved for each architecture evaluated. In terms of the control variable, considering the powertrain model described in previous sections, and especially the energy balance in the DC bus (see *figure 17*), results in:

$$P_{dem} = P_{batt} + P_{FC} \qquad \textit{(Eq. 30)}$$

The battery (P_{batt}), the FC (P_{FC}), or a combination of both can provide the electrical power necessary for the motor to propel the vehicle (P_{dem}). Because the evolution of P_{dem} is solely dependent on the driving cycle, the electrical power demanded (or delivered) to the battery (P_{batt}) may be calculated using the FC power as the control variable ($u = P_{FC}$).

$$P_{batt} = P_{dem} - u \quad \text{(Eq. 31)}$$

Concerning the optimization objective, the fuel consumption (H_2) has been chosen as cost to be minimized. Considering the chosen control variable and optimization criteria, the problem can be formally defined as finding the control law $u(t)$ over time t that minimizes the cost:

$$J = \int_{t_0}^{t_f} P_f(u(t), t)dt \quad \text{(Eq. 32)}$$

where P_f is the fuel (H_2) power consumed as a function of the control variable (u), which in this case is the FC's electrical power. It's worth noting that, because P_f is proportional to fuel consumption, lowering the Eq. will naturally lower fuel consumption.

Because of the univocal relationship between u and P_f, the only state in the system is the energy stored in the battery (E_b), which has the dynamic equation:

$$\dot{E}_b = -P_b \quad \text{(Eq. 33)}$$

being P_b the change in the state of energy of the battery (which is positive when the battery is depleted and negative when the battery is charged).

Finally, because grid charging is not considered and all energy must come from the FC, the net battery charge variance in a long enough cycle should be zero in order to assess battery charge maintaining and to allow a fair comparison of the powertrains considered. This is considered in the optimization problem as follows:

$$\int_{t_0}^{t_f} P_b(u(t), E_b(t), t)dt = 0 \quad \text{(Eq. 34)}$$

The global optimization issue stated in integrated Eqs. can be solved as a series of local optimization problems using Pontryagin's Minimum Principle. The PMP specifically specifies that if u^* and $E^*{}_b$ are the optimal control and battery energy trajectories across the driving cycle, then:

$$H(u^*, E_b{}^*, \lambda^*, t) \leq H(u, E_b{}^*, \lambda^*, t) \forall u \in U, t \in [t_0, t_f] \quad \text{(Eq. 35)}$$

Where H is the Hamiltonian function which can be defined as:

$$iH = P_f - \lambda \dot{E}_b = P_f(u(t), t) + \lambda(t) P_b(u(t), E_b(t), t) \quad \text{(Eq. 36)}$$

The co-state λ has no dimensions because P_f and P_b share the same units. The evolution of λ is identified by PMP as a variation of the Hamiltonian (H) regarding the state (E_b):

$$\dot{\lambda} = \frac{\partial H}{\partial E_b} \qquad \textit{(Eq. 37)}$$

$$\dot{\lambda} = \lambda \frac{\partial P_b}{\partial E_b} = \lambda P_{batt} \frac{\partial \left({}^{P_b}/_{P_{batt}} \right)}{\partial E_b} \qquad \textit{(Eq. 38)}$$

The battery efficiency is represented by the ${}^{P_b}/_{P_{batt}}$ ratio. Because the battery parameters (open circuit voltage and internal resistance) are relatively unaffected by fluctuations in E_b, λ can be assumed constant for the system under consideration (Serrao L, 2009). As a result, the optimization issue is reduced to selecting the right constant value of λ that meets the constraint (Eq. 34).

As a result, the OC problem is reduced to iteratively determining the value of that fulfils the charge-sustaining condition (Eq. 34). Previous studies (Novella, 2021) provide a more detailed description of the EMS optimization algorithm.

For the purposes of this study, the restrictions on $—di/dt—$ and i_{min} are imposed using step functions that affect the cost function J. The Hamiltonian function, which must be minimized at each time step, is thus replaced by:

$$H = P_f - \lambda \dot{E}_b + L_1 \qquad \textit{(Eq. 39)}$$

where L1 is the limiting function that raises the cost function value to infinity for control variable u (current density) values that are outside the imposed bounds at each time step, causing the EMS optimizer to discard the operation at these points.

$$L_1 = \begin{cases} 0 & |di/dt|(t+dt) \leq |di/dt|_{max} \\ \inf & |di/dt|(t+dt) > |di/dt|_{max} \end{cases} \qquad \textit{(Eq. 40)}$$

It should be noted that the operating space of the EMS in terms of current density is [0.01, 1.3] and depending on the driving cycle imposed on the vehicle under study and the operating conditions, this operating range will be optimised as will be seen in the following sections of the analysis.

To summarise the energy control mode in our FC + battery system, the following summary table shows the basis of the EMS:

Energy management main characteristics		
Control input (u)	FC power	$P\mathrm{FC}$
State	Energy in the battery	E_b
Objective	Fuel minimization	Eq. 41
Constraint	Charge sustaining	Eq. 34
Algorithm	PMP	

Table 1: *EMS main characteristics*

3.3. Development of the mean values model

The computational cost is frequently a constraint for analyses that require a large number of simulations. To conduct this kind of study, it is necessary to simulate multiple designs using the Design of Experiments technique. A WLTC driving cycle simulation with all FCREx systems takes around 4 hours, hence the sizing study will take roughly 10 months. The FC system was simplified to a mean values model to save computational costs. This model (Luján JM, 2019), (Guardiola C, 2014), which is frequently utilized in ICE research, interpolates linearly between previously determined points with a low error rate. The total and mean values models were expected to differ due to the steady character of the model, especially given the slow thermal dynamics of FCs that affect their transient performance.

Despite the deviation, this approach was based on a validated model of an FC stack integrated into a BoP whose air management strategy was optimized under different pressure, temperature, and stoichiometry conditions. As a result, the simplified model could reproduce actual FC system operation with simplified dynamics, yielding much higher fidelity results than other approaches in which the entire FC system was oversimplified to a single polarization curve without considering the BoP power demand and inefficiencies associated with driving cycle conditions. Because the FC system is always operating in pseudo steady conditions, the inefficiencies associated with transient operation, such as slow thermal dynamics, are not considered in the mean values model. Nonetheless, the deviation was relatively low and was accepted to reduce the computational cost per case from 4 h to 50 s.

3.4. Simulation process

Two simulation and calculus software tools were utilized to represent the physics involved in the suggested model during the completion of this project. GT-Suite v2020 and MATLAB Simulink were the applications used in this project.

In the first place, GT-Suite is a popular 0D–1D modelling program in the automotive sector. As a result, it can produce high-fidelity mathematical solutions using energy, momentum, and mass conservation equations combined with empirical correlations. Because they can give trustworthy findings at a cheap computing cost, 0D–1D modelling software is ideal for sizing and optimization studies. However, they must be calibrated and validated with experimental data, especially for FC systems.

On the other hand, GT-Suite was connected to MATLAB Simulink to perform the energy management strategy optimization where Simulink is a block diagram environment for designing systems with multi-domain models, simulating them before implementing them on hardware, and deploying them without having to write code. The combination of GT-Suite and MATLAB Simulink can be seen in next figure:

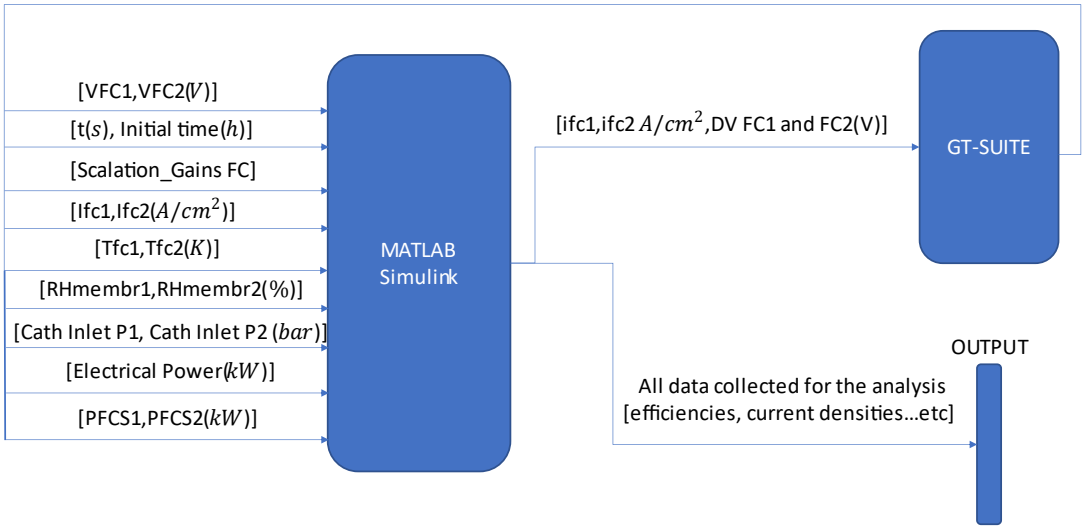

***Figure 19**: Combined models block diagram*

A set of simulations taking into account the WLTC 3b cycle (figure 20) were performed once the modelling platform was built, incorporating the FC vehicle model and sub models, the EMS optimizer, and the FC stack degradation model. The impact of the EMS limits on H2 usage and overall FC system durability was then determined using these simulations. The inferior limit in terms of dynamic limitation was set to 0.001 A/cm2 s and the upper limit for the minimum current density constraint was set to 0.1 A/cm2 from early simulations in order to get sufficient resolution in the results for the analysis. The simulations specified in the simulation matrix (table below) were performed once the extreme restrictions were imposed.

Dynamic $(A/cm^2 \cdot s)$	**0.1**	**0.01**	**0.001**
0.1	1.1	1.2	1.3
0.01	2.1	2.2	2.3
0.001	3.1	3.2	3.3

***Table 2**: Dynamics simulation matrix*

The simulation methodology followed has been based on running the simulation of the matrix of cases below for each combination (80+160, 120+120, 100+140).

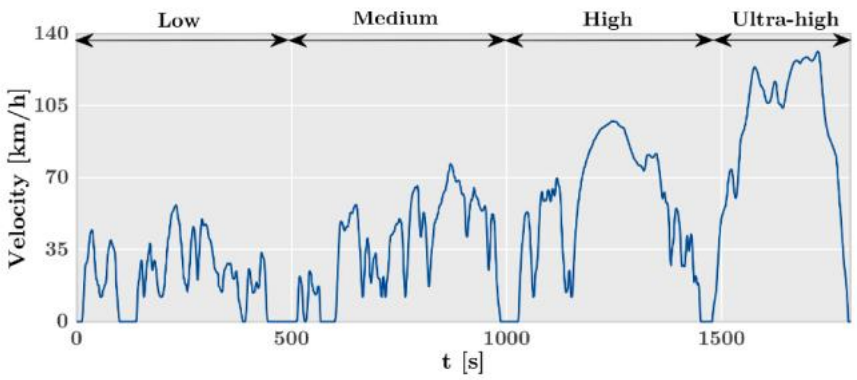

***Figure 20**: WLTC 3b driving cycle velocity profile.*

3.5. Optimization of Performance

The methodology followed to reach this optimization was to test different dynamics strategies for different hydrogen FC power combinations. Starting from the multi hydrogen FC model described above and already implemented in the GT-POWER program with its corresponding coupling with the Simulink program, the process carried out to study the different hydrogen FC combinations was as follows:

The control strategy for the energy consumed by the multi-FC system was put as a basis in the Simulink code in order to carry out the different simulations. These simulations were distinguished by two main elements: the operating dynamics and the power of each stack. The similarities between the different simulations were as follows: same driving cycle for the behavioural study, same physical characteristics of the truck in question (bodywork, chassis, H_2 tank, etc.), restriction that the state of charge (SoC) of the battery in each simulation would always start and end the cycle at the same value 0.3.

As far as energy management is concerned, the strategy is mainly based on finding an optimal "s" throughout the simulation to find the minimum final cost when adding hydrogen consumption plus battery consumption in its operation at compass. This "s" represents the amount of battery consumption to be used in the cycle, i.e., the amount of state of charge to be consumed from the battery.

$$Cost = H_2Consumption + "s" \cdot BatteryConsumption \quad \textit{(Eq. 42)}$$

Once the different simulations have been carried out for each case, the processing of all the data obtained comes into play. This analysis process starts by compiling all the data that MATLAB has collected and capturing it in an Excel spreadsheet. The main data collected for the performance analysis were: the amount of hydrogen consumed at each instant of time during the driving cycle (g/s), the power of each stack at each instant of time (kW), the current density in each stack (A/cm^2), the efficiency of each stack separately, the state of charge of the battery at each instant of time (SoC), the metres travelled by the truck in each driving cycle and finally, the temperature of the stacks in each stack at each instant of time.

To calculate the vehicle consumption ($kg/100km$) the total kg consumed by the battery system during the driving cycle has been divided by the distance travelled during a driving cycle in km and multiplied by 100.

3.6. Optimization of Durability

Because it lowers the FC's maximum power output potential through, among other things, boosting activation, ohmic, and concentration losses, FC degradation must be anticipated. During dynamic operation, when deterioration mechanisms are accelerated due to load cycling, it is particularly crucial to capture these occurrences. For the best energy consumption at any of the powertrain components in vehicle environment, the energy management strategy (EMS) that is in charge of effectively managing the energy flows and power split when an FC and a battery are powering the vehicle at the very same time should be informed of the degradation rate and degraded state of the FC. In light of the fact that increasing electrochemical losses have an impact on energy conversion processes as well as energy management, the development of degradation models that enable on-line degradation prediction is essential. This is because the degradation state of the powertrain components heavily influences the management optimization algorithms' proposed solution. (Huan Li, 2019)

3.6.1. FC Degradation Model

A semi-empirical semi-physical in-house degradation model was used to calculate degradation took it from the paper (Desantes, 2022). It was designed with the assumption that degradation rates scale with electrochemical phenomena and physical conditions (temperature and relative humidity) based

on how degradation indicators (fluoride release rate, platinum grain growth...) evolve as a series of linearly independent functions with current density and operating conditions. The model architecture is made up of three layers that estimate the degradation rate at a given reference current density and then spread it along the polarization curve based on experimental data. Following the sets of equations 42-47, the model estimates the degradation rate by source, differentiating between low-power, natural, high-power, load-change, and start-stop degradation. (Desantes, 2022)

$$\dot{\delta} = \dot{\delta}_{lp} + \dot{\delta}_{lc} + \dot{\delta}_{hp} + \dot{\delta}_{nt} + \dot{\delta}_{ss} \quad \textit{(Eq. 43)}$$

$$\dot{\delta}_{lp} = \dot{\delta}_{lp,\ ref} \cdot \xi_{lp}(i) \cdot \tau(T_{FC}) \cdot \eta(\overline{RH}) \quad \textit{(Eq. 44)}$$

$$\dot{\delta}_{lc} = \dot{\delta}_{lc,\ ref} \cdot \xi_{lc}\left(\frac{di}{dt}\right) \cdot \tau(T_{FC}) \cdot \eta(\overline{RH}) \quad \textit{(Eq. 45)}$$

$$\dot{\delta}_{hp} = \dot{\delta}_{hp,\ ref} \cdot \xi_{hp}(i) \cdot \tau(T_{FC}) \cdot \eta(\overline{RH}) \quad \textit{(Eq. 46)}$$

$$\dot{\delta}_{nt} = \dot{\delta}_{nt,\ ref} \cdot \xi_{nt}(i) \quad \textit{(Eq. 47)}$$

$$\dot{\delta}_{ss} = \dot{\delta}_{ss,\ ref} \quad \textit{(Eq. 48)}$$

Where δ is the voltage fraction loss (1-$V_{degraded}/V_{FC}$), $\dot{\delta}_{X,ref}$ is the reference degradation rate for the degradation source X, and ξ_X, η_X, and τ_X are the scaling functions for the degradation source X that scale the reference degradation rates with the electrochemical phenomena, FC stack temperature and cathode and anode average relative humidity, respectively.

The reference degradation rates are measured in the first layer under reference conditions of current density, temperature, and relative humidity (Pucheng Pei, 2008). To ensure model continuity along the polarization curve, the high-power degradation rate was calibrated to include the effect of natural degradation on the model, which was included as a medium-load degradation. Table below contains the reference degradation rates for this model.

Condition	δ [fraction of V loss]
Low power [/h] ($\dot{\delta}_{lp,\ ref}$)	$1.26 \cdot 10^{-5}$
Load change [/cycle] ($\dot{\delta}_{lc,\ ref}$)	$4.94 \cdot 10^{-7}$
High power [/h] ($\dot{\delta}_{hp,\ ref}$)	$1.03 \cdot 10^{-5}$
Start-stop ($\dot{\delta}_{lp,\ ref}$)	$1.96 \cdot 10^{-5}$

***Table 3**: Reference degradation rates for the FC Degradation model*

These reference degradation rates were determined at T_{FC}~50°C and $\overline{RH}$~80%. Low-power degradation was measured at 0.01 A/cm^2, high-power degradation was measured at 1 A/cm^2,, and load-change degradation was measured with a load-cycle current density amplitude ranging from 0.01

to 1 A/cm^2,. Following the model philosophy of scaling degradation rates through physical trend identification, the functions that comprise layers 2 and 3 were designed to have a value of one at reference conditions, i.e., the conditions under which the reference degradation rates (table above) were measured.

2nd layer: scaling with electrochemical phenomena	
Low power $\xi_{lp}(i) = -0.176 \cdot \ln i + 0.169$	Based on: Membrane degradation: Fluoride release rate change at low voltage (S.Knights, 2012) Catalyst degradation: oxidation of the carbon surface (K. H. Kangasniemi, 2004)
Load change $\xi_{lc}\left(\frac{di}{dt}\right) = \frac{\lvert\Delta i\rvert_{dt}}{2\,\lvert\Delta i\rvert_{ref}}$	For a given time step, degradation scaling with load-change amplitude is used. $\lvert\Delta i\rvert_{dt}$ denotes the variation in current density over a given time step dt, and $\lVert\Delta i\rvert_{ref}$ denotes the load-change amplitude per load-change cycle in (Pucheng Pei, 2008)
High power $\xi_{hp}(i) = \frac{i}{i_{hp}}$	Based on scaling the degradation with the flow of protons through the membrane (electrochemical reaction rate) since at high power there is not significant degradation due to electrochemical phenomena, but it is scaled with temperature. i_{hp} (1 A/cm^2) is the current density at which high-power degradation becomes significant.
Natural $\xi_{nt}(i) = \frac{\dot{\delta}_{hp,\,ref} \cdot \xi_{hp}(i_{hp}) - \dot{\delta}_{lp,\,ref} \cdot \xi_{lp}(i_{lp})}{i_{hp} - i_{lp}} \cdot (i - i_{lp})$	Based on scaling degradation with the flow of protons through the membrane (proportional to i) degradation rate continuity from low-power to high-power conditions is provided.

***Table 4**: Conditions for the refence degradation rates.*

The second layer is used to scale the reference degradation rates via the ξ_X functions based on the current density of the FC stack at each time step. Each time step, these functions are evaluated based on the instantaneous current density and its variation with respect to the previous time step (|di/dt|). Table above contains them, as well as the reasoning behind their development.

$$\tau(T_{FC}) = -5.390 \cdot 10^{-4} T_{FC}^2 + 0.399 T_{FC} - 71.576 \qquad \textit{(Eq. 49)}$$

Similar to τ, η was obtained based on the experiments of Dutta et al. (Dutta, 2010), who investigated the effect of relative humidity on Pt grain size growth rate through voltage cycling at various relative humidity levels. Based on the data from (S.Knights, 2012) (Nengyou Jia, 2009), this degradation mechanism has a direct effect on the electrochemical surface area (ECSA) decrease, which was converted to voltage loss:

$$\eta(\overline{RH}) = 0.10646 e^{0.028 \cdot \overline{RH}(\%)} \qquad \textit{(Eq. 50)}$$

Following the set of equations, all the defined equations are used to calculate the voltage degradation rate at a reference current density of 1 A/cm^2. In accordance with the accelerated degradation tests and subsequent analysis on the polarization curve change performed by (Dario Bezmalinovic, 2015), the effect of voltage degradation along the polarization curve is then spread linearly with current density.

3.6.2. Methodology

Once the degradation model was implemented and adjusted in our FC System model and after all the cases simulations, different data was used to evaluate the durability of the FC stack combinations depending on the dynamic strategy followed. For each of the FCs, a series of variables relating to the degradation of each cell was obtained after finding the optimum of the simulation. The meaning of these variables is basically the variation of the degradation voltage for each of the different driving modes with which the model estimates the degradation rate by source, differentiating between low-power, natural, high-power, load-change, and start-stop degradation.

The durability or life of the stack was calculated using the Department of Energy's end of life (EOL) criteria, which state that an FC stack has reached the EOL when the voltage drops by 10% compared to nominal conditions at a current density of 1 A/cm^2. Specifically, to calculate the life of the FC in terms of kilometres, the voltage variation per kilometre $\frac{\mathrm{dV}}{\mathrm{km}}$ has been calculated by adding the low-power, natural, high-power, load-change variations and dividing them by the distance travelled during the driving cycle and that added to the voltage variation at start-stop multiplied by 2 and divided by the number of kilometres at which our vehicle will stop to refuel hydrogen, which is 400 km:

$$\frac{\mathrm{dV}}{\mathrm{km}} = \frac{\dot{\delta}_{lp} + \dot{\delta}_{lc} + \dot{\delta}_{hp} + \dot{\delta}_{nt}}{cycle\ distance} + \frac{\dot{\delta}_{ss} \cdot 2}{stop\ distance} \qquad \textit{(Eq. 51)}$$

$$Durability = \frac{EOL\ Criterium}{\frac{\mathrm{dV}}{\mathrm{km}}} \qquad \textit{(Eq. 52)}$$

The influence of the change of the operating temperature of the stack has not been analysed in this work because the temperature change was minimal and therefore its influence on the degradation of the stack system was null. This is due to the fact that the BoP and its cooling system maintain the stack temperature at around 80°C.

3.7. Calculation of TCO and LCA

3.7.1. TCO

Alternative drive-technologies that reduce or eliminate a vehicle's carbon footprint usually come at a price. As with any new technology, initial capital cost competitiveness is difficult to achieve. However, in some cases, while the initial cost of a new technology may be high, switching to a new technology may result in lower long-term costs. An investor switching to a new technology, for example, may benefit from increased operating efficiency of the technology's core functionality or a reduction in the annual costs required to power and maintain this technology. A TCO analysis, by combining the initial

purchase cost and annual operating expenditures, provides a fair assessment of the cost effectiveness of alternative vehicle drive-technologies over their entire lifetime. (Bessie Noll, 2021)

The total cost of ownership, often abbreviated as TCO, is an analysis focusing on the cumulative total of costs contributed by each stage of a product's life cycle (Shiyue Mao, 2021). Unlike the passenger vehicle sector, the heavy-duty truck sector is focused on the total cost of the vehicle over its entire operational lifetime (Coalition, 2010) (Coalition, 2020). Heavy-duty vehicles have a higher daily utilization rate, have longer lifetimes, and operate in predictable, often pre-determined, strategically optimized routes. Because of the high operating costs, fleet owners and commercial transportation businesses rely heavily on the TCO as a cost evaluation metric. (Bessie Noll, 2021)

TCO analyses are far more common in the passenger vehicle sector than in the commercial vehicle sector, according to the literature. Several passenger vehicles studies examine and compare specific technical variations within a given drive-technology (for example, degrees of hybridization in hybrid-electric vehicles). Others have compared the TCO cost-benefits of hybrid vs. full electric vehicles, as well as 'regular' cars. According to the findings of these studies, the TCO of electric passenger vehicles may be comparable to, if not lower than, that of conventional vehicles by 2025. (Bessie Noll, 2021).

3.7.1.1. Methodology

The TCO equation proposed by (Bessie Noll, 2021) paper has been chosen as the basis for this study because of its intensive research on the various TCO studies carried out in recent years and because it fills the gaps in the knowledge that these studies have not been able to fill. Nevertheless, several modifications or considerations have been made to simplify the calculation: Infrastructure Costs are counted inside the Fuel Costs, and it is not going to use in the equation Driver Wages and Insurances. Consequently, the formula on which the work has been done and with which the TCO has been calculated is:

$$TCO = CAPEX \cdot CRF + OPEX \quad \textit{(Eq. 53)}$$

$$CAPEX = Energy\ Storage + Powertrain + Rest\ of\ Truck \quad \textit{(Eq. 54)}$$

$$OPEX = Tolls + Fuel\ Costs + O\&M \quad \textit{(Eq. 55)}$$

$$CRF = \frac{i(1+i)^N}{(1+i)^N - 1} \quad \textit{(Eq. 56)}$$

Where TCO is the total cost of ownership per truck $(€/truck)$, $CAPEX$ is the capital expenditure or the initial purchase cost of the vehicle, $OPEX$ is the operating expenditure or the total operating cost of the vehicle and CRF is the capital recovery factor where i is the discount rate and N is the lifetime of the vehicle $(years)$. The $Energy\ Storage$ refers to the battery pack cost and the H_2 tank storage (Yvonne Ruf, 2020). The $Powertrain$ is mainly the FC System cost (Bessie Noll, 2021) and the electric motor cost while the $Rest\ of\ Truck$ is typical cost of the truck without the powertrain (Yvonne Ruf,

2020). The TCO results as can be seen in the formula are presented in the form of total euros at the end of the truck's lifetime even though most of the data collected were prices per year.

Regarding the system boundaries of the TCO calculation it should be noted that the study has focused on a time span from 2022 through 2025 to 2030 and the data obtained can be geographically located in Europe. For each of these years, the necessary data has been collected for the above-mentioned parameters of the formula. The table below shows the main data used for the TCO calculation together with their functional units and their respective sources:

		2022	2025	2030	
	Units	**Niche**	**Rather-niche**	**Rather-mass**	**References**
FC System	$€/kW$	860	374	200	(Yvonne Ruf, 2020)
Electric Motor Cost	$€/kW$	35	32.5	30	(Bessie Noll, 2021)
Small Battery Cost	$€/kWh$	364	262	204	(Yvonne Ruf, 2020)
H_2 Tank 350 bar Price	$€/kgH_2$	292	258.5	225	(Yvonne Ruf, 2020)
Road Toll	$€/km$	0.17	0.17	0.17	(Yvonne Ruf, 2020)
Maintenance Cost	$€/km$	0.11	0.11	0.11	(Yvonne Ruf, 2020)
Discount Rate (i)	%	0.17	0.17	0.17	(Bessie Noll, 2021)
Green Hydrogen cost	$€/kg$	5	3	2	(McKinsey&Company, 2021)
Blue Hydrogen cost	$€/kg$	2	1.8	1.7	(McKinsey&Company, 2021)
Grey Hydrogen cost	$€/kg$	1.5	1.6	1.75	(McKinsey&Company, 2021)
Electricity mix Price	$€/kWh$	0.237	0.232	0.228	(Eurostat, 2022)

***Table 5**: TCO main data.*

	Units	**Truck Daily Route**	**References**
4x2 Rigid Truck	$km/year$	92,500	(Yvonne Ruf, 2020)
Days/Year Travelled	$day/year$	250	(Yvonne Ruf, 2020)
Kilometres Travelled in a day	km	370	Assumption
Kilometres of battery use in a day	km	71.6	Assumption
Kilometres of FC use in a day	km	298.4	Assumption
Battery consumption without FCS	kWh/km	0.1368	Assumption
Use of the battery	%	19%	Assumption
Use of the FC System	%	81%	Assumption

***Table 6**: TCO main daily route data.*

As far as the cost part is concerned, most of them have been taken from the total cost of ownership study carried out by the European Union (Yvonne Ruf, 2020) because no more reliable source or scientific study could be found. In relation to hydrogen fuel prices depending on their source of origin (green, blue, and grey), data from the report by McKinsey & Company together with the Hydrogen Council have been used, as the assumptions on which they were based were in line with this work. (Company, 2021). To clarify what green, blue, and grey hydrogen means, it is necessary to look at the definitions: green hydrogen is produced by electrolyzing water with clean electricity generated by renewable energy sources such as solar or wind power. Electrolysers use an electrochemical reaction to split water into its constituents, hydrogen, and oxygen, while emitting no carbon dioxide. Blue hydrogen is primarily produced from natural gas through a process known as steam reforming, which combines natural gas and heated water in the form of steam. The by-product is carbon dioxide, but the output is hydrogen. As a result, carbon capture and storage (CCS) is required to trap and store this carbon. Finally, grey hydrogen is produced from natural gas, or methane, via steam methane reformation without capturing the greenhouse gases produced.

In terms of durability, the FC system has the life imposed by the results of the calculation of the durability of each FC combination that has been done in the durability analysis section, so for each case the FC system will have a life. In relation to this it is worth mentioning that the life of the average truck that has been chosen is 8 years of life. Shorter lifetimes than European average (ACEA Driving mobility for Europe, 2022) has been chosen due to eliminate the need for battery replacement. Based on expert interviews, that battery replacement for heavy-duty trucks will last 7 to 8 years and battery warranty for light- and medium-duty trucks will last 6 to 8 years. (Bessie Noll, 2021)

The data table shows some of the considerations necessary to perform the calculation and then shows the actual route that the truck will take every day, chosen based on the range results obtained in the durability and performance study. The data for this daily route selected for the TCO and LCA study are shown in table 6 and in figures 21-23 it can be seen in the description how the daily route is powered.

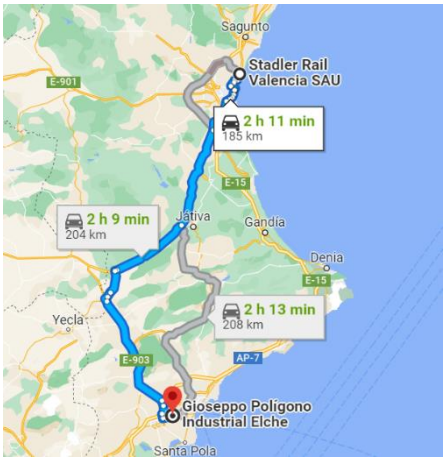

***Figure 21**: A route of 370km has been chosen as the route for the truck's daily logbook (round trip).*

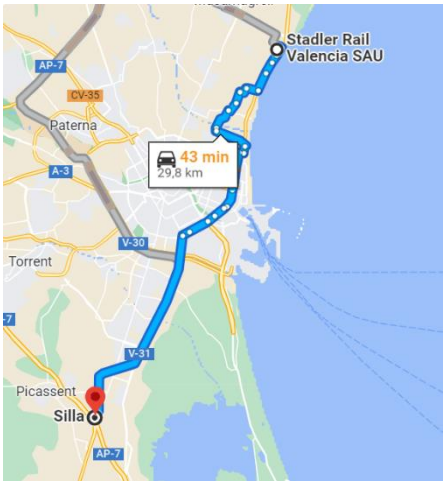

Figure 22: *Journey in Valencia from the industrial estate to the motorway (AP-7) during which the truck will be powered by the battery alone.*

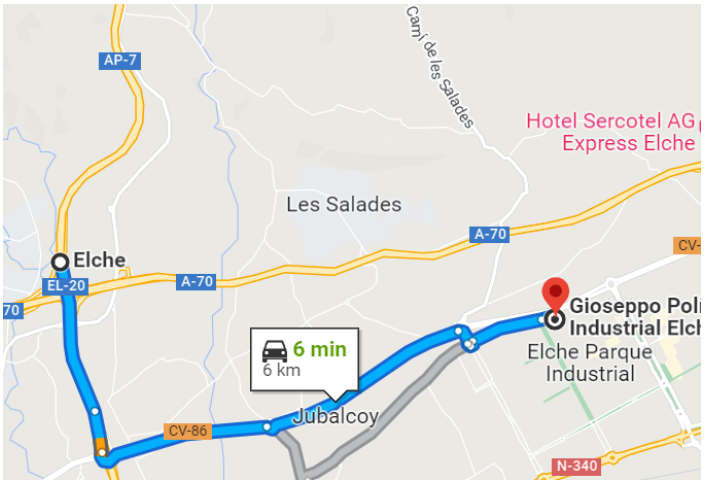

Figure 23*: Journey in Elche from the industrial estate to the motorway (AP-7) during which the truck will be powered by the battery alone.*

3.7.2. LCA

This study aims to be a cradle-to-grave cycle assessment that considers state-of-the-art automotive technologies, such as CI ICE fuelled with Diesel, battery electric systems and obviously our hydrogen FC system with the goal of extending the analysis provided by the already available scientific literature and evaluating the EU objectives of increasing the renewable energy share in the electricity mix. This study focuses on heavy duty transport because this has the greatest impact on NO_X and CO_2 emissions when considering the road transport sector. (Novella, 2020)

3.7.2.1. Methodology

Fuel production, vehicle production, vehicle disposal, and operating cycles should all be included in a cradle-to-grave assessment of a given transportation system. The next table lists the engine technologies and their respective fuels that were investigated in this study.

Figure 24 depicts the system boundaries for each individual cycle, as well as the system inputs and outputs. They are those that correspond to a cradle-to-grave LCA, i.e., from the extraction of raw materials through the use of energy and fuel through the vehicle's disposal and recycling. GREET® was used to compute waterborne, solid waste, and other atmospheric emissions such as SO_X, but they were not included in this study.

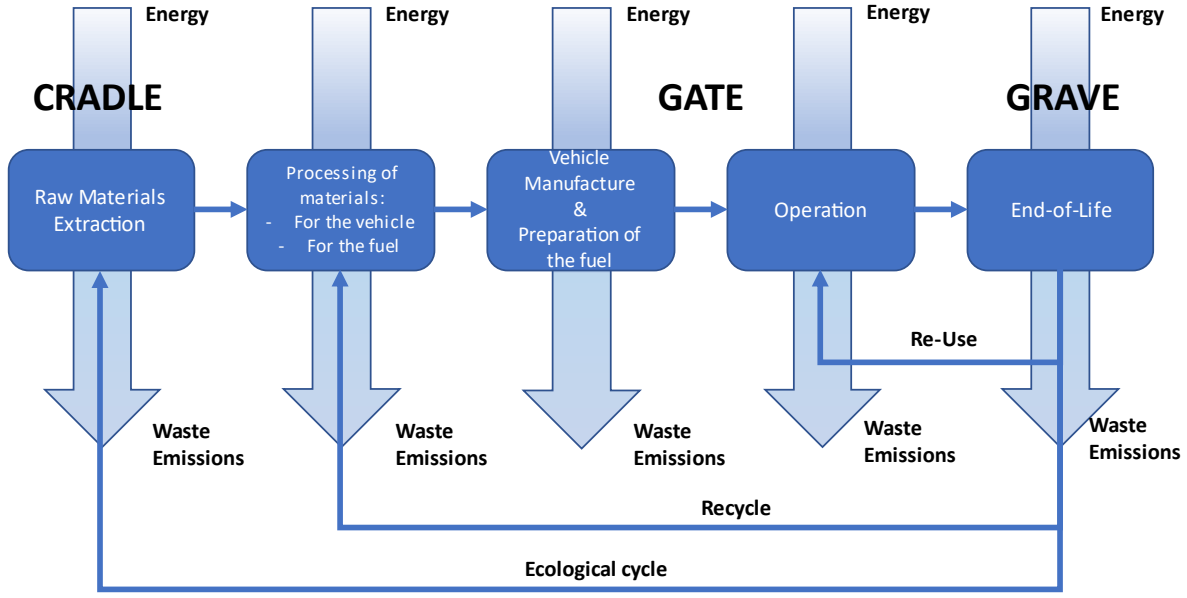

Figure 24: *System boundaries and elementary flows for the cradle-to-grave process considering electrolysis, SMR and SMR with CCS as the H_2 production pathways.*

Regarding the functional units used for this study in the fuel production cycle was the MJ of fuel because several fuels with different lower heating values and densities were compared. The emissions were calculated per manufactured vehicle during the vehicle production cycle. Finally, the functional unit in the cradle-to-grave cycle, which included the previous cycles as well as vehicle operation, was the life of each truck, with 750,000 km as the average common life, and the production of a unit of the considered heavy-duty FCV. (8 years). (Pier Giuseppe Anselma, 2021)

Global Warming was the only impact category considered in this LCA study. GHG were calculated by accounting for CO_2, CH_4, and N_2O gaseous emissions. Their GWPs are 1, 28, and 265 kg CO_2 equivalent (IPCC, 2012).

Regarding data sources, all the data extracted for this study comes from different sources of LCA programs such as: GREET® model version 2019 from the Argonne National Laboratory, GaBi and kg CO_2 eq. data extracted from the paper that is based this study. (Novella, 2020). For the calculation of this LCA it has also been necessary to use some of the data implemented for the calculation of the TCO.

The table below shows the main data scenario used for the LCA calculation together with their functional units and their respective sources:

		Scenario		
	Units	**EU-28 2020**	**EU-28 2030**	**Source**
E-motor emissions	$[kg\ CO2\ eq./kg]$	2.67	2.53	(GaBi, s.f.) electricity mix + (GREET, s.f.)
E-motor specific power	$[kW/kg]$	4		
E-motor power	$[kW]$	350		
E-motor manufacturing emissions	$[kg\ CO2\ eq.]$	233.48	221.47	
Battery NMC622 emissions	$[kg\ CO2\ eq./kg]$	11.91	11.27	(GaBi, s.f.) electricity mix and baseline emissions + (GREET, s.f.)
Battery energy density	$[kWh/kg]$	0.168		(GaBi, s.f.)
Battery capacity	$[kWh]$	73.2		
Battery manufacturing emissions	$[kg\ CO2\ eq.$	5,189.74	4,909.36	
FC system emissions	$[kg\ CO2\ eq./kg]$	2.80	2.56	(GaBi, s.f.) + (GREET, s.f.)
FC system specific power	$[kW/kg]$	0.65		DoE FC system targets for 2020
FC system power	$[kW]$	240		
FC system manufacturing emissions	$[kg\ CO2\ eq.]$	1,033.99	943.75	
H_2 tank emissions	$[kg\ CO2\ eq./kg]$	9.54	8.16	(GREET, s.f.)
H_2 tank gravimetric capacity	$[kg\ H2/kg\ tank]$	0.044		(DoE, s.f.)
H_2 in tank capacity	$[kg]$	32.09		
H_2 tank manufacturing emissions	$[kg\ CO2\ eq.]$	6,959.2	5,953.8	
Heavy-duty vehicle body	$[kg\ CO2\ eq.]$	17,179.0	17,179.0	(GaBi, s.f.)
Total cradle-to-gate emissions	$[kg\ CO2\ eq.]$	30,595.4	29,207.3	

***Table 7**: Main data for the LCA calculation.*

Once all this data is collected, the methodology for calculating the LCA was to play with this data and the consumption and durability data obtained from the previous studies of the different stack system configurations with the different cases of dynamics used for the performance of the stack. For example, the number of times the FCs were replaced in the vehicle is a very important factor to calculate the carbon footprint of the truck while the hydrogen consumption of each FC is a very important input when calculating the total emissions during the entire vehicle operation phase.

4. ANALYSIS OF RESULTS

This section covers the analysis of the results obtained along the completion of this study for all FC systems combinations applied.

4.1. Performance analysis

The EMS optimizer's ability to manage the energy flows produced by the FC system is directly impacted by the limitation of —di/dt— when the drive cycle is in operation. Given that the boundary condition for the EMS is to maintain the battery SOC at the same level at the start and end of the driving cycle (charge sustaining), any restriction on the EMS that prevents the FC system from operating at its best must be made up for by increasing the power generated (current density) under other operating conditions. As a result, restricting the dynamics of the FC system affects not only the circumstances that the FC system is unable to attain because of EMS limits, but also the entire cycle. This suggests that the current density evolution throughout the driving cycle, not just in the high-dynamics period, will be considerably impacted.

The 120+120kW FC system has been taken as the basis for the performance analysis. The next figure shows how current density change depending on the restrictions imposed to the EMS:

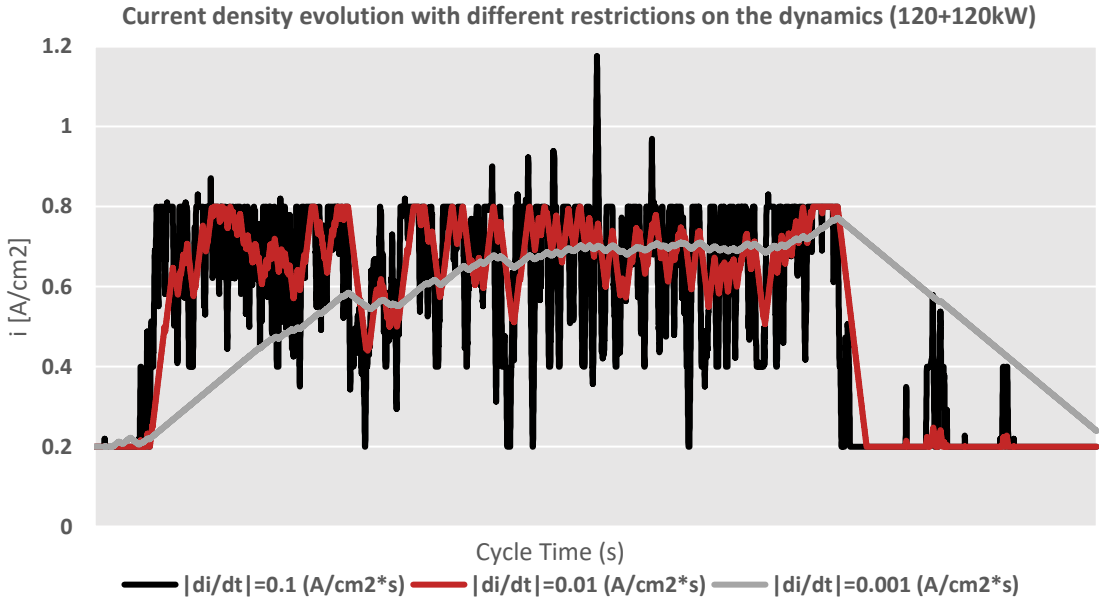

***Figure 25**: Current density evolution with different restrictions on the dynamics (120+120kW).*

It can be clearly seen in the figure how the EMS chooses as the range of current densities of maximum operating efficiency one comprised between 0.2 and 0.8 A/cm^2. Analysing this figure, it is noticeable that the more you restrict the control dynamics, the less variability in the evolution of the current density during the cycle is observed, i.e., the less jumps and peaks appear as it behaves in a more linear way. And this has a direct effect in that the EMS will not be able to keep up with the demand of the electric motor if it demands very dynamic loads. To demonstrate this, the following figure shows how in the case in which the FCs work with moderate dynamics both (0.01-0.01) try to follow the demand of the electric motor but having a current density that varies very little and evolves almost constantly the power of the FC that is directly related to the current density cannot follow the demand of the

electric motor. This demand from the electric motor that cannot be met by the FC system due to the restriction in dynamics is supplied by battery power.

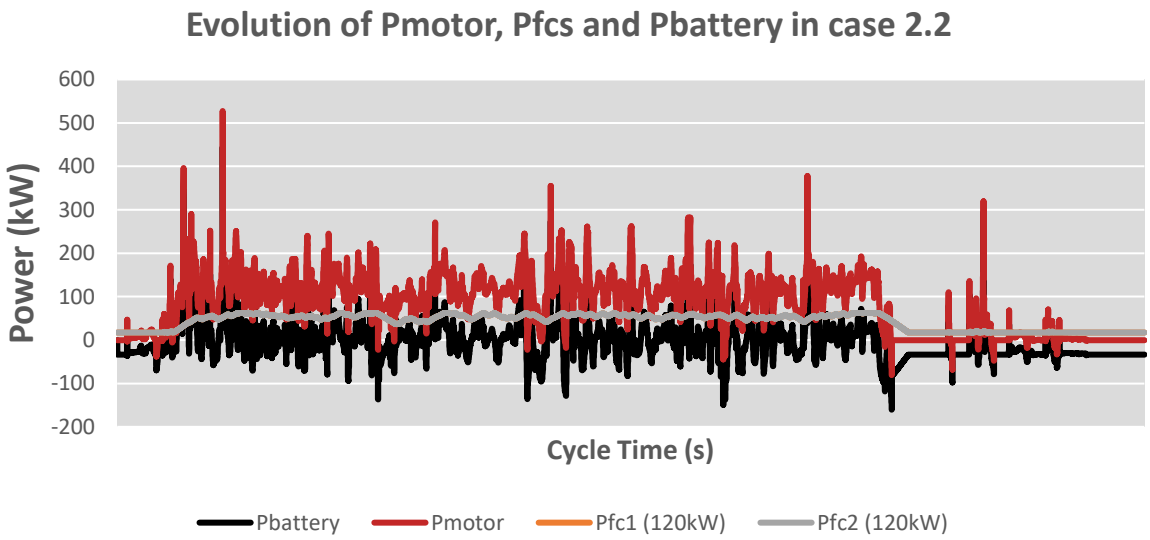

***Figure 26**: Evolution of the electrical power demand, FC system power and Battery power in case 2.2.*

This behaviour, which has been explained, is repeated in the other FC combinations (80+160kW) and 100+140kW) and has a clear influence on the consumption of the system, which is sought to be minimized due to the main objective of the EMS.

Then this analysis has focused on a comparison of the fuel consumption of different combinations of 120+120 kW, 80+160 kW and 100+140 kW multi-stack systems plus the different dynamics strategies with which the hydrogen FC/battery combination has worked. To carry out this analysis, it is necessary to know how a hydrogen FC behaves according to the dynamics used in its control strategy, and an easy and simple way to observe how it behaves is through a series of graphs showing the consumption in kilograms of hydrogen per 100 kilometres. The 120+120 kW FC combination is first analysed:

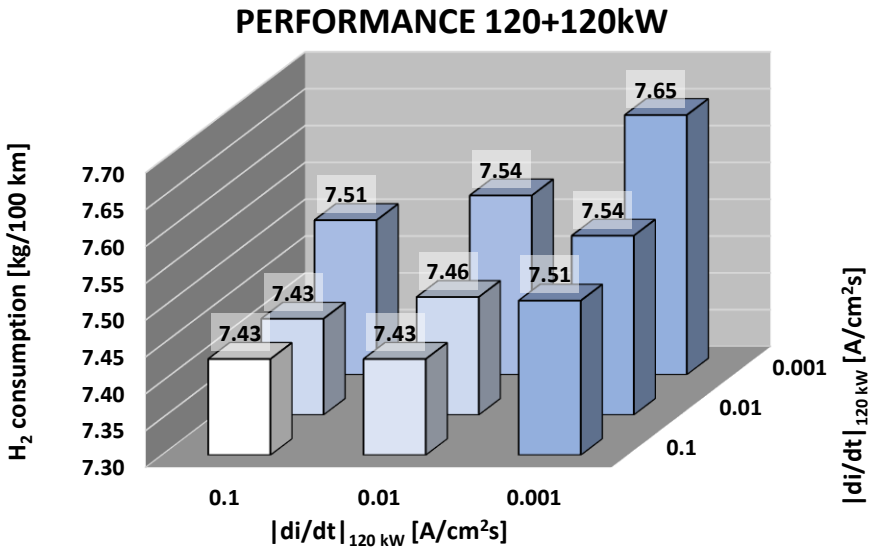

***Figure 27:** Performance of the 120+120kW design in every dynamic case.*

This graph tells us that the increase in hydrogen consumption of the system is directly related to how much you restrict the EMS control dynamics. The lower the dynamics (di/dt < 0.1 A/cm2*s), the higher the hydrogen consumption. This is directly related to the above explanation of the current density evolution, where it has been confirmed that the lower the dynamics, the less the current density varies and therefore is not able to follow the changing electric motor demand. This causes the system to behave in suboptimal conditions and causes the consumption to increase. Having explained this, one way to support this argument is to graph the efficiency of the system for each combination of dynamics. One would expect from the EMS strategy that the lower the hydrogen consumption of the system, the higher the efficiency of the system, as EMS aims to achieve the lowest consumption. Let's take a look at the graph below:

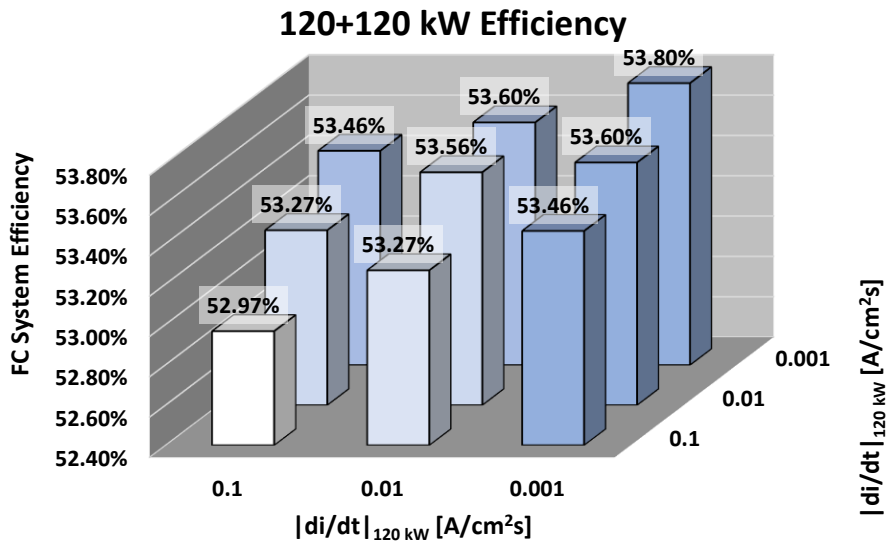

***Figure 28**: Efficiency of the 120+120kW FC system operation.*

Having looked at the graph, it can be confirmed that the previous assumption was not correct and that the efficiency is increasing each time you restrict the dynamics further. But how can this be explained? Well, in order to explain such a behaviour, it is necessary to plot the battery usage for the same cases:

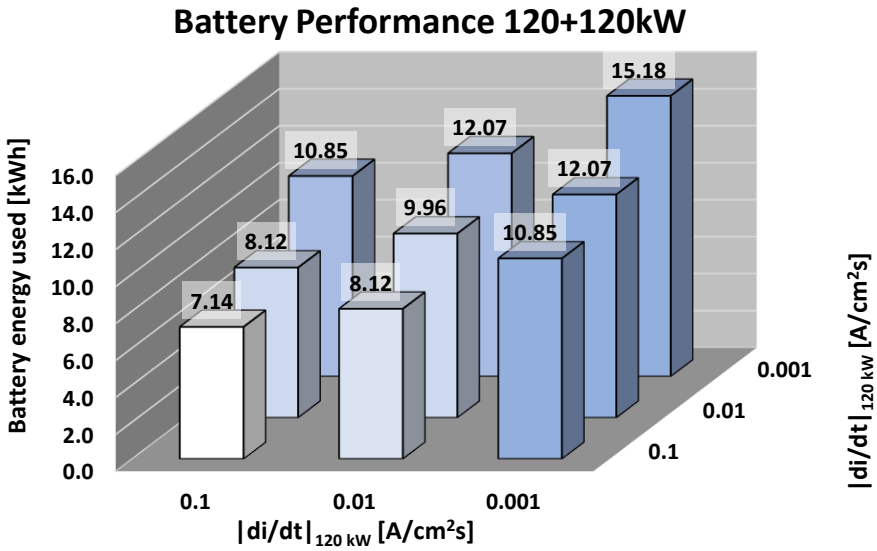

***Figure 29**: Battery performance in the 120+120kW system design in every dynamic case.*

It has also been observed that the lower the control dynamics of the FC system, what happens is that the battery tends to be used more. This means that after that higher usage you have to recharge it and that is additional energy that you have to produce through the FCs. But why does the efficiency tend to be higher the more the battery and the FC system is used? Well, because the system operates under less dynamic, more restrictive conditions, then the system operates under suboptimal conditions because it cannot follow the power demand of the electric motor, i.e., it cannot go into dynamic mode following the variations in the demand of the electric motor. So, what the EMS does is to choose to operate the FC systems in the regions where there is higher system efficiency (figure 30). In the end, what is happening is that within the polarisation curve the system is working with a slow evolution of current density until it leads to high load so what happens is that more time is spent in the high efficiency area of the curve where the system operates in the best current density range. The consumption still increases due to the high utilisation of the battery which means that it is recharged using the FC system. To summarise, as the control strategy is suboptimal (slow dynamics), the battery is discharged more and as the state of charge of the battery has to be equal at the beginning and at the end this causes the FC system to use more hydrogen producing more power thus increasing the consumption, but all this while operating in the higher efficiency zone. The following figure shows the optimal power distribution of the FC system as a function of current density. With this it can understood the range where the EMS tries to operate when the dynamics are so restricted and thus at least achieve the highest possible efficiency with the range of current densities shown.

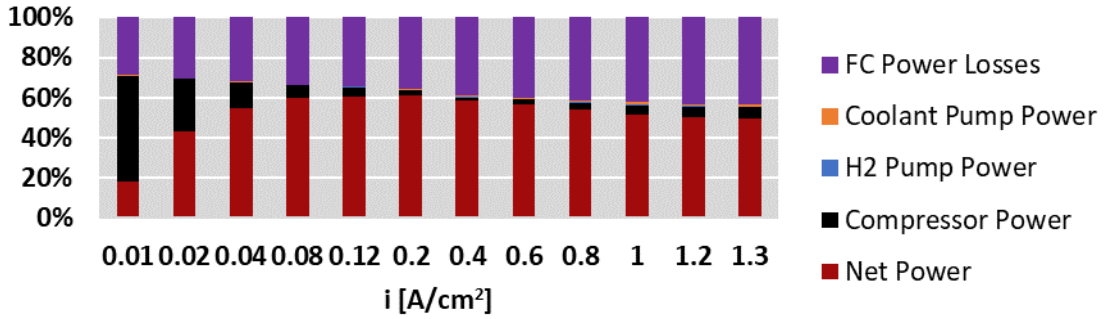

Figure 30: *FC system optimum power distribution as a function of the current density. (Novella, 2021)*

Having explained the trend for the 120+120 kW combination, it has been observed that the other 2 FC combinations also follow this trend. But the difference between the different combinations is in the absolute consumption values that are achieved depending on the selected architecture. To observe this, the consumption graphs of 80+160kW and 100+140kW will be plotted in order to compare how much they differ from each other and to see which combination achieves the most optimal consumption.

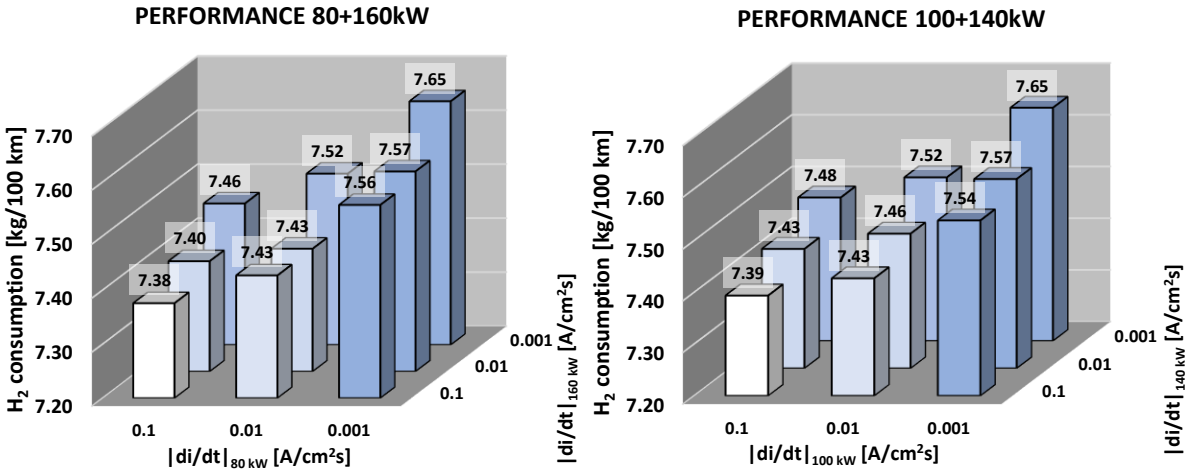

Figure 31*: Performances of the 80+160kW and 100+140kW designs in every dynamic case.*

Looking at the consumption trend of both combinations, it can be stated that they behave in the same way as the consumption of the 120+120 kW system. Furthermore, it can be said that the absolute values do not change in an exaggerated way as the total consumption variations in kg/100km are maximum around 3%.

To conclude this part of the analysis of the performance results, the following table shows the optimal results in terms of consumption for the different designs studied:

Design	Optimal Dynamic	Consumption (kg/100km)
120+120	1.1	7.4305
80+160	1.1	7.3757
100+140	1.1	7.3972

***Table 8**: Performance optimum results*

4.2. Durability analysis

The analysis of the durability of the FC systems that have been studied is clearly reflected in the behaviour of the degradation rates explained in the methodology and which have such an influence on the degradation model. The influence of changing the dynamics can be seen clearly in the various degradation rate sources. This effect of change in control dynamics has been highlighted especially in the degradation rates of load change and start-stop. To demonstrate this, the 120+120 kW FC system will be analysed first.

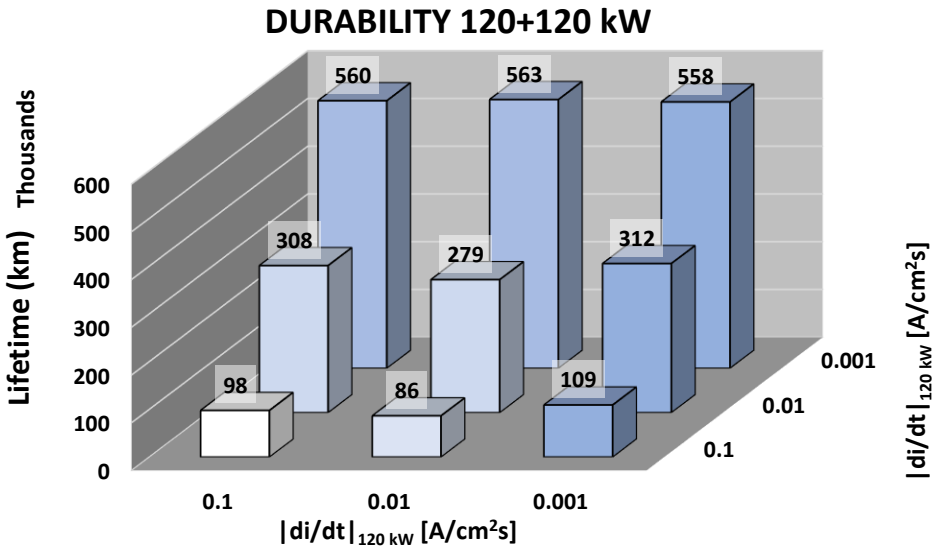

***Figure 32**: Durability of one of the FCs of the 120+120kW system design.*

These durability results refer to the durability of one of the FCs of the 120+120 kW system. Only a few results have been given, as the two FCs have the same power ratings and perform in the same way. Looking at the durability results in the graph, it can be seen how the constraining dynamics on the control of the system cause the stack life to increase considerably. This could be explained by knowing that by restricting the dynamics, the FC system does not behave dynamically to follow the demand of the electric motor and makes the battery work harder, so the FC system degrades less because it does

not operate with very high-power peaks and current densities, but almost constantly. But apart from this explanation, it is necessary to refer to how the degradation rates discussed above influence the durability of the system. While the start-stop degradation rate remains constant as the dynamics vary, the load-change varies. But both are the most influential when calculating durability as they are the parameters with the highest value. The following figure shows how the load change varies according to the simulated dynamics and the direct relationship with the durability of the system. The behaviour of the degradation rates that have been calculated for each stack have followed the same trends that have been observed in one of the articles where this technology is studied, and which summarizes in a very concrete way how the degradation rates evolve as you increase the restriction in the dynamics. (J.M. Desantes, 2022)

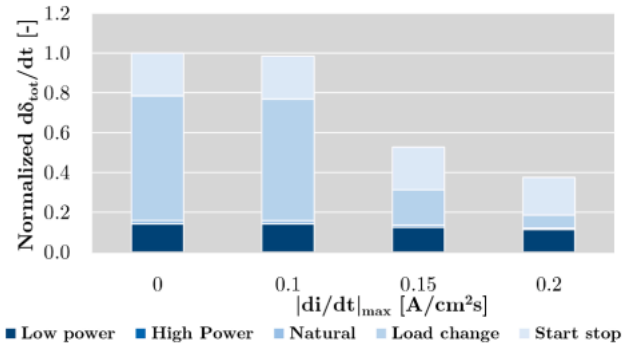

Figure 33: Normalized total degradation rate variation with —di/dt—max segmented by source.

Where it can be observed that the smaller you make the dynamics the higher degradation rates you get. And the most prominent or that most influence the result of degradation of the stack are those of Load change and start-stop.

This studied durability changes are now going to be analysed depending on the combinations of FCs you use. For this purpose, graphs will be drawn showing the durability achieved by each combination for each dynamic case and then it will be shown in which cases the maximum durability is achieved and which combination is the optimum in terms of achieving more km of life for the FC.

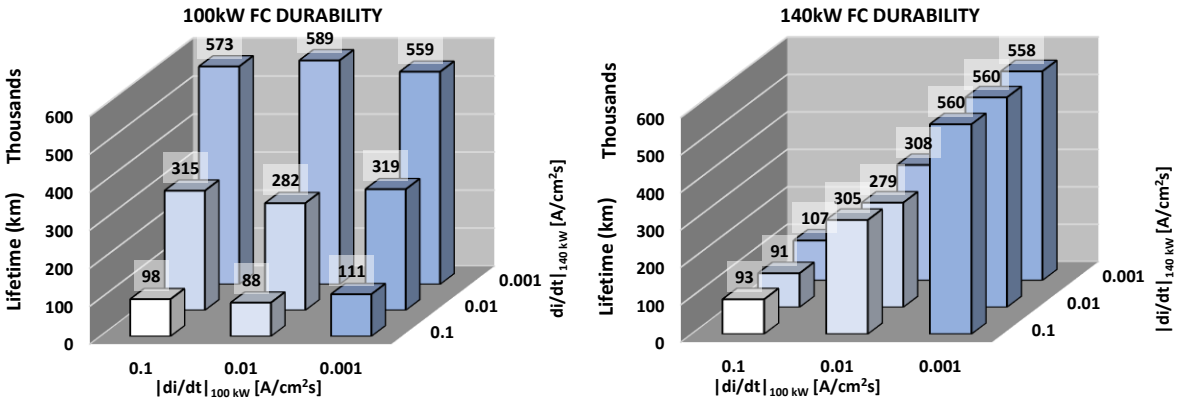

Figure 34: Durabilities of the FCs of the 100+140kW system design in every dynamic case.

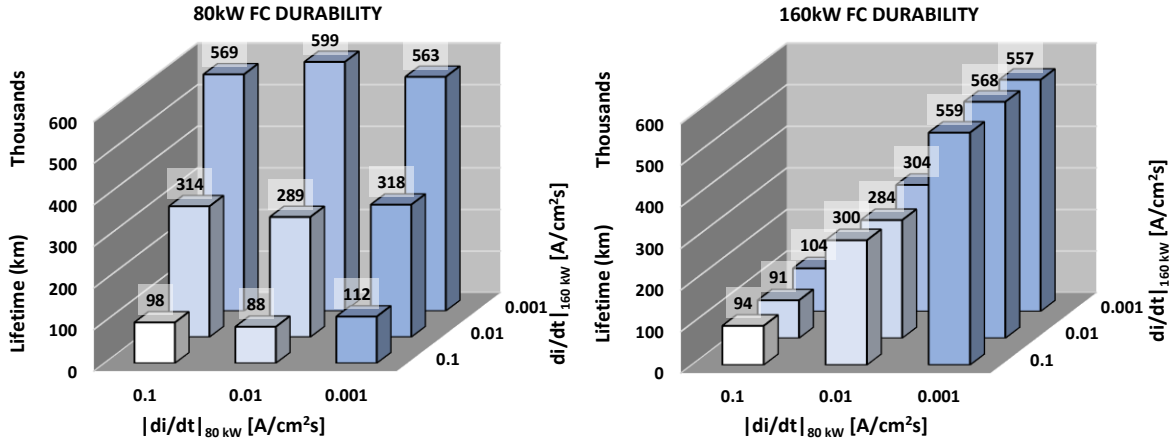

***Figure 35**: Durabilities of the FCs of the 80+160kW system design in every dynamic case.*

Once the durability graphs have been analysed, in all designs the optimum durability value is found in case 3.2 of the dynamic's simulation matrix. A detailed study was carried out to clarify why the optimum was found in 3.2 and not in 3.3, as the more restricted the dynamics the less degradation, and from the analysis of the data it was found that the current density values for the 3.2 case were smaller. As the values are smaller than in 3.3, the FCs deliver less power and therefore put less demand on the system and degrade less.

On the other hand, the maximum durability value obtained was in the 80+160kW design, specifically in the smallest FC with the 3.2 dynamic. The value of this optimum was 598,649 km of stack life, 6% higher than that of 120kW in the same dynamic case.

Finally, a summary table will be presented with the durability results obtained together with the optimal designs:

Design	Optimal Stack (kW)	Optimal Dynamic	Durability (km)
120+120	120	3.2	562,898
80+160	80	3.2	598,649
100+140	100	3.2	588,998

***Table 9**: Summary results of durability optimums*

4.3. TCO analysis

The TCO analysis has been structured in 3 different cases as it was felt that this would give a broad overview of the costs involved in using the different FC combinations, the different energy control strategies and the different types of hydrogen fuel used.

Case 1: two FC system combinations will be compared in two different scenarios: in the first scenario the TCO results divided into CAPEX and OPEX will be compared in 2022 and 2030, using green hydrogen. In the second scenario, the mentioned combinations will be compared, but this time with the grey hydrogen as fuel.

- 1st Scenario:

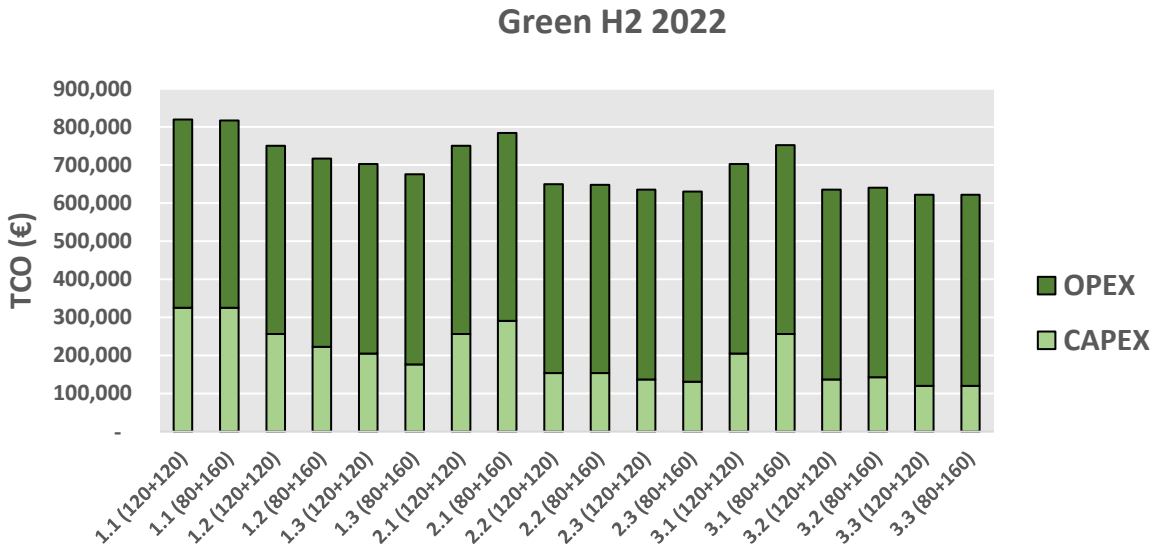

***Figure 36**: CAPEX and OPEX results of the 120+120kW and 80+160kW system designs in every dynamic case with 2022 data using green H2.*

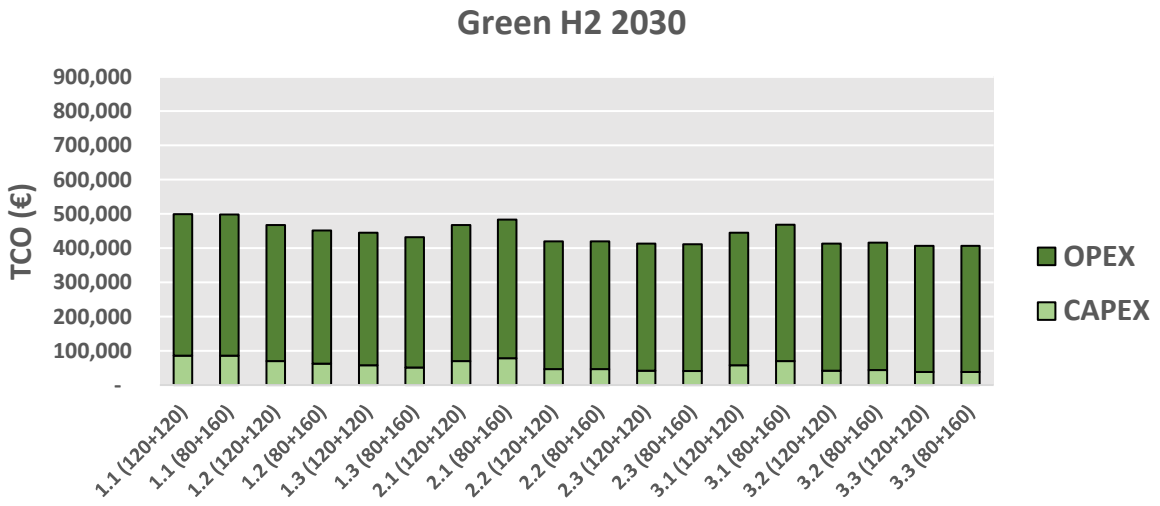

***Figure 37:** CAPEX and OPEX results of the 120+120kW and 80+160kW system designs in every dynamic case with 2030 data using green H2.*

Looking at how TCO evolves from 2022 to 2030, CAPEX is reduced much more than OPEX, by 70% and 20% respectively. This shows the strong influence of the price change of the FC system. However, there is also a strong influence of the hydrogen price since the absolute OPEX values are higher than the CAPEX values. With regard to absolute TCO values and their evolution over time, price ranges for 2022 of [600,000, 800,000] and for 2030 of [400,000, 500,000] can be observed. Talk about differences between combinations 1.1(120+120) 1.1(80+160)

- 2nd Scenario:

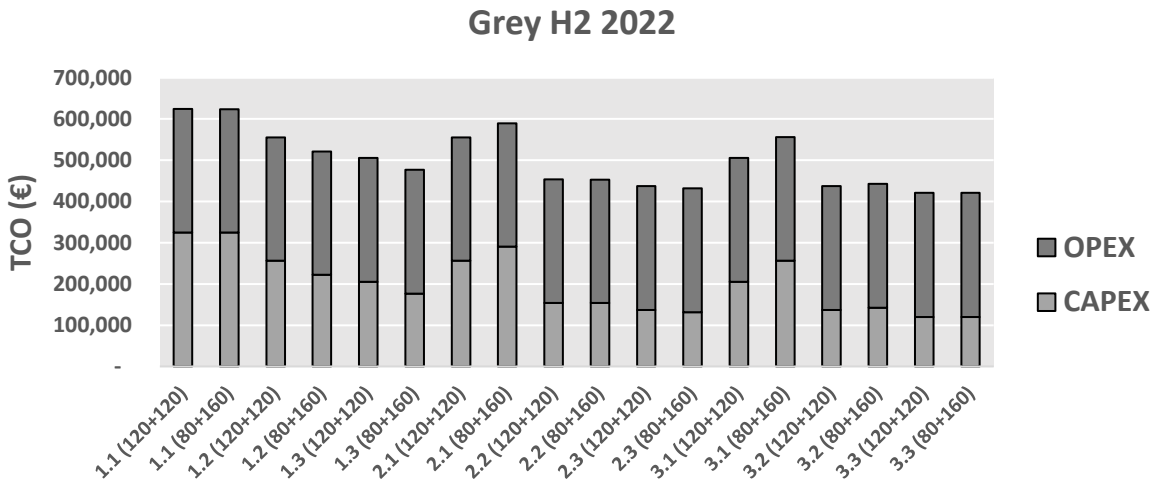

***Figure 38**: CAPEX and OPEX results of the 120+120kW and 80+160kW system designs in every dynamic case with 2022 data using grey H2.*

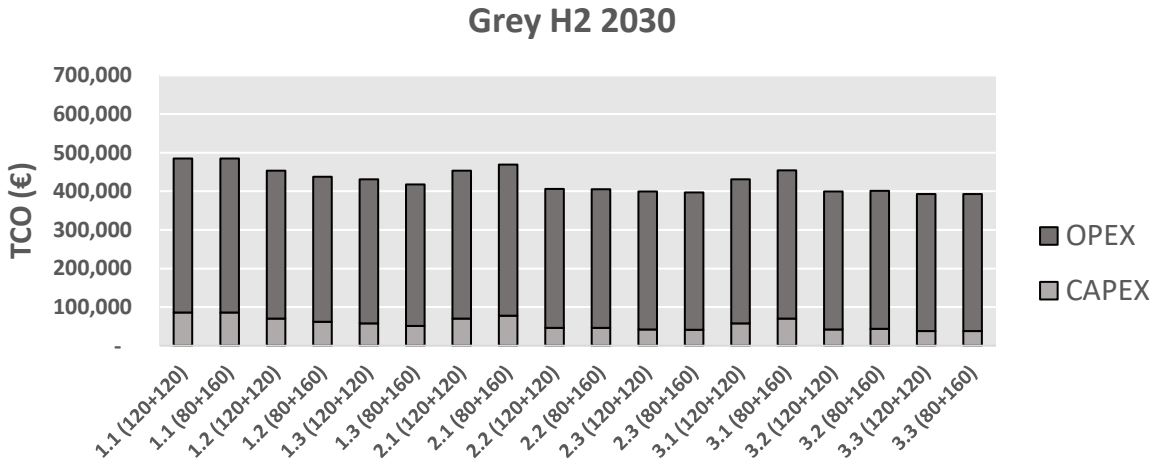

***Figure 39**: CAPEX and OPEX results of the 120+120kW and 80+160kW system designs in every dynamic case with 2030 data using grey H2.*

Analysing as in the previous scenario, here it can be seen that CAPEX behaves exactly the same since it is not influenced by fuel prices. What is important here is to see the evolution of OPEX, which behaves inversely than in the previous scenario and is basically due to the increase in the price of grey hydrogen due to CO2 taxes and increases in natural gas prices. This increase in OPEX is around 20% for all cases. With regard to absolute TCO values and their evolution over time, price ranges for 2022 of [400,000, 600,000] and for 2030 of [400.000, 500.000] can be observed.

Case 2: In this case, the TCO reduction from 2022 to 2030 will be analysed for each combination of FC and dynamics for the different types of hydrogen used as fuel.

Green Hydrogen TCO reduction (from 2022 to 2030)			
Dynamic	**120+120**	**80+160**	**100+140**
1.1	49.58%	49.55%	50.21%
1.2	47.10%	45.68%	46.40%
1.3	44.99%	43.69%	44.35%
2.1	47.10%	48.38%	47.76%
2.2	42.43%	42.40%	42.43%
2.3	41.60%	41.31%	41.46%
3.1	44.99%	47.12%	46.44%
3.2	41.60%	41.88%	41.72%
3.3	40.75%	40.75%	40.75%

***Table 10**: TCO reduction from 2022 to 2030 for each combination of FC and dynamics using GREEN hydrogen.*

Blue Hydrogen TCO reduction (from 2022 to 2030)			
Dynamic	**120+120**	**80+160**	**100+140**
1.1	39.21%	39.24%	40.34%
1.2	34.81%	32.20%	33.54%
1.3	30.73%	28.11%	29.45%
2.1	34.81%	37.14%	36.00%
2.2	25.85%	25.86%	25.85%
2.3	23.95%	23.28%	23.61%
3.1	30.73%	34.79%	33.52%
3.2	23.95%	24.59%	24.28%
3.3	21.91%	21.91%	21.91%

***Table 11**: TCO reduction from 2022 to 2030 for each combination of FC and dynamics using BLUE hydrogen.*

Grey Hydrogen TCO reduction (from 2022 to 2030)			
Dynamic	**120+120**	**80+160**	**100+140**
1.1	36.05%	36.10%	37.34%
1.2	31.04%	28.04%	29.59%
1.3	26.31%	23.25%	24.82%
2.1	31.04%	33.71%	32.40%
2.2	20.65%	20.68%	20.65%
2.3	18.38%	17.58%	17.97%
3.1	26.31%	31.01%	29.54%
3.2	18.38%	19.15%	18.78%
3.3	15.91%	15.91%	15.91%

***Table 12**: TCO reduction from 2022 to 2030 for each combination of FC and dynamics using GREY hydrogen.*

According to the tables above, the fastest control dynamics result in the highest TCO reduction for the three types of hydrogen. This means that the weight of the hydrogen price in the TCO calculation is much more important than the weight of changing the FC system more frequently over the truck's lifetime.

Case 3: Finally, two summary tables will be made for 2020 and 2030 showing for each design the optimal dynamics in terms of costs.

Scenario 2022						
	Green		**Blue**		**Grey**	
Design	**Optimal Dynamic**	**Cost**	**Optimal Dynamic**	**Cost**	**Optimal Dynamic**	**Cost**
120+120	3.3	622,215 €	3.3	450,031 €	3.3	421,334 €
100+140	3.3	622,146 €	3.3	450,003 €	3.3	421,313 €
80+160	3.3	622,146 €	3.3	450,003 €	3.3	421,313 €

***Table 13**: Summary table with optimal TCO designs for 2022.*

Scenario 2030						
	Green		**Blue**		**Grey**	
Design	**Optimal Dynamic**	**Cost**	**Optimal Dynamic**	**Cost**	**Optimal Dynamic**	**Cost**
120+120	3.3	368,661 €	3.3	351,443 €	3.3	354,313 €
100+140	3.3	368,634 €	3.3	351,420 €	3.3	354,289 €
80+160	3.3	368,634 €	3.3	351,420 €	3.3	354,289 €

***Table 14**: Summary table with optimal TCO designs for 2030.*

It can be noticeable that the cost optimum is achieved in the most constrained dynamics since the weight of the cost of the FC system is much higher and has more influence than the cost of the hydrogen consumed. In other words, it is worthwhile to operate the system with restricted dynamics so that the lifetime of the FCs is as long as possible and so that they do not have to be replaced as

often as with less restricted dynamics, and also because the influence of the increase in consumption when restricting the dynamics is very small, since the consumption per km varies very little in comparison.

It should also be noted that the TCO for green H2 in 2022 is well above the TCO for blue and grey H2, but that by 2030 it will be competitive and a very low-emission alternative with a minimum cost premium of about 5% compared to the use of blue and grey H2.

4.4. LCA analysis

The LCA analysis will be carried out following the TCO analysis methodology but this time looking at the final life cycle emissions of the vehicle instead of the costs. Therefore, 2 different cases of analysis will be presented where different aspects of the results will be highlighted.

Case 1: in the next graphs it is showed the total cradle-to-grave emissions at the end of life of our truck with the 120+120kW FC system design, with current prices for battery production, FC system, vehicle body production, H2 tank production and electric motor production, for the different types of hydrogen and the different designs.

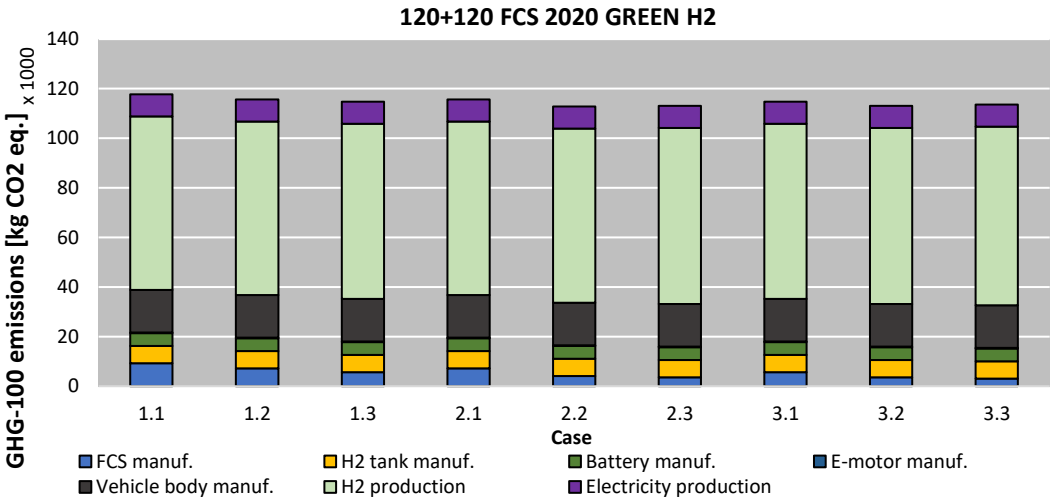

Figure 40: Total cradle to grave GHG-100 emissions of the 120+120kW FC system design in every dynamic case using green H2 with 2020 data divided by emission source.

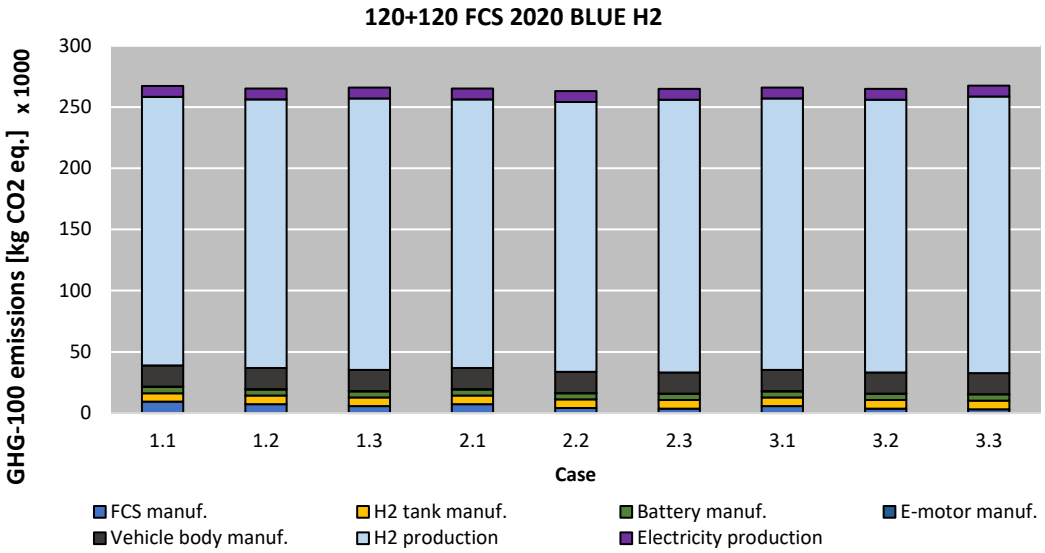

Figure 41: *Total cradle to grave GHG-100 emissions of the 120+120kW FC system design in every dynamic case using blue H2 with 2020 data divided by emission source.*

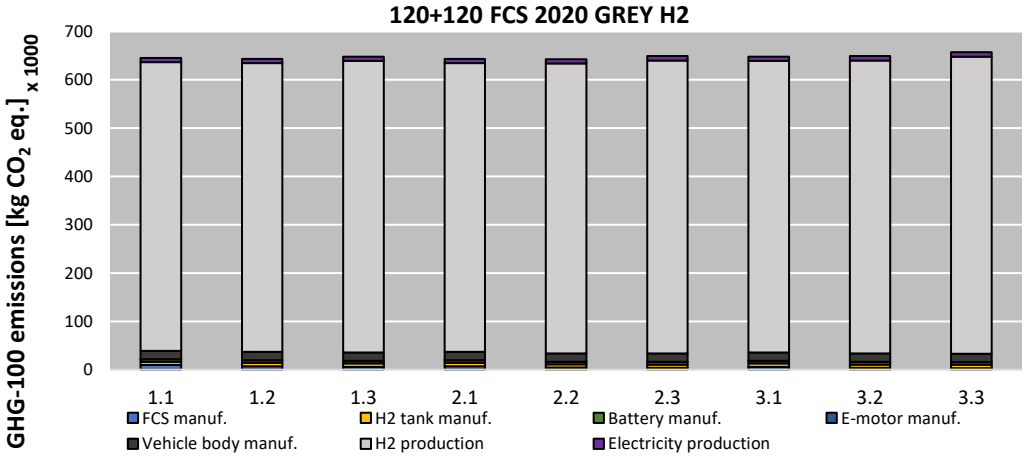

Figure 42*: Total cradle to grave GHG-100 emissions of the 120+120kW FC system design in every dynamic case using grey H2 with 2020 data divided by emission source.*

It should be noted that the large amplitude of the source of emissions related to hydrogen production is due to the long vehicle life imposed in the previous sections. A lifetime of 750,000 km greatly increases the emissions from hydrogen production. But if we go back to the data in the LCA emissions table, we can see how the main parameters in terms of emissions are: the battery, the FC system, H2 tank and vehicle body manufacture apart from the emissions from hydrogen production. The change in the way hydrogen is produced greatly influences the total cradle to grave emissions but due to the long lifetime of the vehicle a fair comparison with other emission sources cannot be made. Let's see in the following case how these emissions behave when the system design is changed.

Case 2: In this case, the total LCA results for each FC system design and for each case of dynamics depending on the type of hydrogen used will be presented in summary tables.

Total cradle to grave emissions [kg CO2eq.] 120+120kW Design									
2020	**1.1**	**1.2**	**1.3**	**2.1**	**2.2**	**2.3**	**3.1**	**3.2**	**3.3**
GREEN H2	117,692	115,625	114,820	115,625	112,801	113,075	114,820	113,075	113,578
BLUE H2	267,177	265,109	265,901	265,109	262,881	264,846	265,901	264,846	267,531
GREY H2	645,425	643,358	648,187	643,358	642,635	648,880	648,187	648,880	657,086

***Table 15**: Total cradle to grave emissions [kg CO2eq.] 120+120kW Design for each type of H2 in 2020 scenario.*

Total cradle to grave emissions [kg CO2eq.] 80+160kW Design									
2020	**1.1**	**1.2**	**1.3**	**2.1**	**2.2**	**2.3**	**3.1**	**3.2**	**3.3**
GREEN H2	117,176	114,558	114,407	116,411	112,491	113,148	115,917	112,990	113,561
BLUE H2	265,557	263,974	266,448	265,365	261,908	265,445	266,029	264,212	267,477
GREY H2	641,013	642,048	651,164	642,272	639,986	650,808	645,862	646,855	656,938

***Table 16**: Total cradle to grave emissions [kg CO2eq.] 80+160kW Design for each type of H2 in 2020 scenario.*

Total cradle to grave emissions [kg CO2eq.] 100+140kW Design									
2020	**1.1**	**1.2**	**1.3**	**2.1**	**2.2**	**2.3**	**3.1**	**3.2**	**3.3**
GREEN H2	117,982	115,068	114,672	116,161	112,804	113,212	115,542	112,893	113,561
BLUE H2	266,796	264,469	266,358	265,687	262,891	265,461	265,954	264,091	267,477
GREY H2	643,348	642,506	650,177	644,040	642,663	650,704	646,551	646,675	656,938

***Table 17**: Total cradle to grave emissions [kg CO2eq.] 100+140kW Design for each type of H2 in 2020 scenario.*

Total cradle to grave emissions [kg CO2eq.] 120+120kW Design									
2030	**1.1**	**1.2**	**1.3**	**2.1**	**2.2**	**2.3**	**3.1**	**3.2**	**3.3**
GREEN H2	101,218	99,331	98,533	99,331	96,730	96,913	98,533	96,913	97,286
BLUE H2	250,816	248,929	249,728	248,929	246,924	248,799	249,728	248,799	251,356
GREY H2	628,951	627,064	631,900	627,064	626,564	632,718	631,900	632,718	640,793

***Table 18**: Total cradle to grave emissions [kg CO2eq.] 120+120kW Design for each type of H2 in 2030 scenario*

Total cradle to grave emissions [kg CO2eq.] 80+160kW Design									
2030	**1.1**	**1.2**	**1.3**	**2.1**	**2.2**	**2.3**	**3.1**	**3.2**	**3.3**
GREEN H2	100,791	98,360	98,118	100,069	96,473	96,959	99,573	96,857	97,271
BLUE H2	249,285	247,890	250,274	249,137	246,004	249,371	249,798	248,194	251,304
GREY H2	624,628	625,850	634,875	625,931	623,969	634,619	629,518	630,722	640,649

***Table 19**: Total cradle to grave emissions [kg CO2eq.] 80+160kW Design for each type of H2 in 2030 scenario*

Total cradle to grave emissions [kg CO2eq.] 100+140kW Design									
2030	**1.1**	**1.2**	**1.3**	**2.1**	**2.2**	**2.3**	**3.1**	**3.2**	**3.3**
GREEN H2	101,509	98,827	98,374	99,819	96,733	97,019	99,218	96,770	97,429
BLUE H2	250,437	248,341	250,175	249,459	246,934	249,384	249,745	248,083	251,462
GREY H2	626,876	626,264	633,879	627,698	626,592	634,511	630,228	630,552	640,806

***Table 20**: Total cradle to grave emissions [kg CO2eq.] 100+140kW Design for each type of H2 in 2030 scenario*

Having all the LCA results in the above tables and having analysed them, it can be stated that:

- Firstly, the optimum of minimum emissions is achieved in the case where the control dynamics of the two FCs of the system operate moderately (2.2). This means that, compared to previous consumption and durability analyses, where minimum consumption was achieved for fast dynamics and maximum durability for slow dynamics, the LCA finds a middle ground. In other words, the design optimum works with a trade-off between consumption and durability where minimum emissions are achieved.
- Secondly, it is worth noting the clear difference between an LCA calculated with green hydrogen and another with grey hydrogen, where a difference in emissions of around 500 tonnes of CO2 eq. is quantified in absolute value.
- Thirdly and lastly, it is worth noting that the reduction of total emissions over time is more pronounced in the LCA calculated with green H2 than with blue and grey H2. This is seen in that the reduction in emissions from 2020 to 2030 with H2 green produced is around 15%, while for H2 blue and grey it is 7% and 3% respectively.

For the latest analysis, the emissions of this new technology have been compared with those of today's heavy-duty diesel and electric vehicles in 2022. To do this, cradle-to-grave emissions data had to be collected for a vehicle with similar characteristics to ours and with the same lifespan. These data have been acquired from the official website of Volvo trucks in which you could make a kind of footprint calculation of the different trucks and models they have in the company. (UK, s.f.)

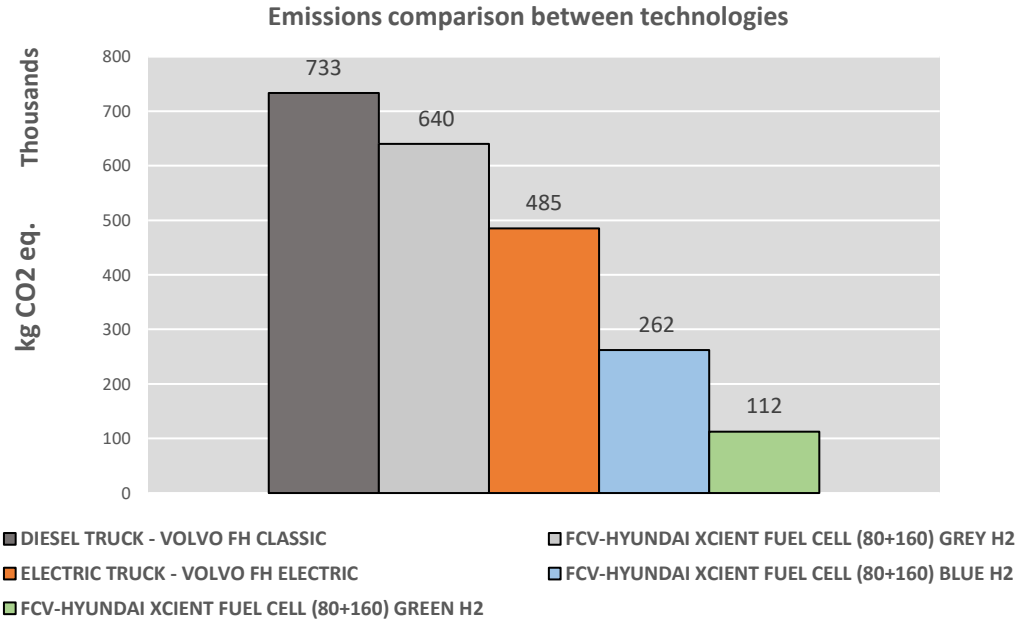

***Figure 43**: CO2 eq. emissions comparison between FC, battery propulsed and diesel truck technologies.*

What this graph basically tells us is that FC technology applied to heavy-duty is today the one with the best CO2 footprint over the lifetime of the truck if green hydrogen is used and produced for its operation followed by the same using blue hydrogen. Then comes the battery-only electric truck in third place, followed by the FC system truck using grey hydrogen and at the bottom of the ranking of the best truck technologies in terms of minimum emissions is the traditional diesel internal combustion engine truck. The large difference in emissions over the lifetime of a diesel truck and a truck powered by green H2 is worth noting which is around 600 tonnes of CO2 eq. It should be noted that this analysis has been a mere estimation and exact data has not been taken due to lack of information.

5. CONCLUSIONS

This chapter summarizes the conclusions that may be drawn from the analysis of the integration of multiple FC systems in heavy-duty vehicle architecture, answering the main objectives set out at the beginning of the paper. The project's planned objectives have been accomplished, and this part reviews the effort and outcomes.

- From the analysis of the Performance and Durability can be concluded that lifetime of the FC system changes far more than fuel consumption. This translates to shifting the design balance toward durability rather than fuel consumption, as it is much more cost-effective to replace the fuel cell system every 500,000 km and spend 3% more hydrogen than to replace the FCs every 100,000 km for only saving very little consumption. Therefore, when choosing the best FC system design, it is necessary to opt for EMS control dynamics that are not so detrimental to the durability of the battery and that operate in the most efficient way in terms of minimum consumption. These dynamics correspond to the moderate-slow ones.
- From the analysis of the TCO results it can be said that although the cost reduction over time is higher with fast dynamics for all designs, i.e. the total absolute value cost of TCO is minimal in slow dynamics, case 3.3 of the simulation matrix. In other words, because the weight of the cost of the FC system is much higher and has more influence than the cost of the hydrogen consumed, the cost optimum is achieved in the most constrained dynamics. It can also be concluded that, by 2030, the TCO for green H2 is already competitive and a very low-emission alternative with a minimum additional cost of about 5% when compared to the TCO for blue and gray H2.
- In the LCA analysis it has been concluded that when the control dynamics of the two FCs run moderately, the lowest possible emissions are reached (2.2). This indicates that the LCA finds a midway ground when contrasted to earlier consumption and durability assessments, where least consumption was attained for fast dynamics and maximum durability for slow dynamics. In other words, the design that produces the lowest amount of emissions while balancing consumption and durability. It can also be stated that using green H2 in this technology reduces the total cradle to grave CO2 eq. emissions of the truck's life cycle by around 500 tonnes compared to using grey H2, which implies a huge difference in the carbon footprint. And finally, it has been concluded that the FC system in heavy-duty has much lower CO2 eq. emissions (500 tons) than those of a conventional heavy-duty diesel and that is why this technology is so interesting to achieve the Net Zero objectives set by the European Union, since the weight of the heavy-duty transport sector in emissions is considerable.

6. BUDGET

This section serves to provide a cost analysis of the project's implications in terms of labour hours and resources used.

6.1. Distribution of working hours

This project started on February 1st and ended on June 30th which gives 108 working days. With a daily workload of 5 hours during the week results in 540 hours of work. This 540-hour total includes hours spent reviewing literature, getting used to and learning about new simulation software, meetings with the tutor, hours spent calculating and analysing the models, and finally writing the thesis. The computational hours required to complete the simulations must be added to this. This is divided into two categories. The first were simulations for optimizing the FC system, which meant 9 different simulations, one for each of the three FC System combinations. It accounted for a total of 40,5 hours with a mean duration of 1.5 hours per simulation. The following simulations were directly related to degradation adjustment. This setting had a load of 2 hours for each FC combination to reach the parameters needed to calibrate the degradation model. Once calibrated, the simulation of the different cases for each combination had to be carried out again with a total of 0.5 hours per case because the optimum performance had already been found in the first part of the simulations. Therefore, all the above gives a total of 100 hours of simulation considering the repetition of simulations as a refinement process.

Assignment	Time ($hours$)
Literature Research	110
Learning the new simulation software	20
Model & Analysis Development	160
Meetings	30
Simulations	100
Thesis writing	180
Total	**600**

***Table 21**: Distribution of working hours*

6.2. Labour costs

The expense is determined by the number of hours worked by everyone involved in the project's completion. This includes the PhD professor, PhD assistant, and master's graduated engineer. The PhD professor served as a tutor and assisted with the project's completion. The PhD assistant assisted in guiding the graduated engineer who completed the project. It first displays the cost per unit of time (€/h) of each category, and then evaluates the cost regarding the working hours that each person brings to this specific task. The average hour salary of each involved in the project is:

- PhD professor: results in 16.74 €/h.
- PhD assistant: results in 14.61 €/h
- Graduated engineer: results in 4.15 €/h.

Employee	Time (hours)	€/hour	Total Cost €
PhD professor	10	16.74	167.4
PhD assistant	30	14.61	438.3
Master's Graduated engineer	600	4.29	2,574.0
		Total	**3,179.7 €**

***Table 22**: Labour costs.*

6.3. Equipment costs

The section that follows investigates the cost per usage of software licenses and the equipment required to run them. This quantifies the cost of the programs used, which is typically measured in cost per year, and converts it to cost per hour, as well as the total cost of the material used divided by the estimated use of the material.

Licence	Time (hours)	€/hour	Total cost (€)
MATLAB Simulink	200	0.03	6
GT-Suite	150	0.34	51
Microsoft Office	300	0.01	3
Equipment			
Laptop	600	0.022	13.2
		Total	**73.2 €**

***Table 23**: Cost of use of computer equipment and simulation software licences.*

6.4. Operational costs

The operational costs are the expenses incurred because of the actions required to complete a task. Because no other resources were used in the project, the cost of electricity will be the main in this case. Because the project was purely analytical and consisted solely of simulations, there was no need to visit the CMT labs to perform any experiments, so the total costs do not compute.

The price of electricity has varied considerably during the months in which the work has been carried out due to the gas supply crisis as a result of the war in Ukraine. Depending on the month, the price per megawatt has changed, so OMIE's monthly reports have been consulted for the average daily market price for that month: 200.47 €/MWh in February, 283.26 €/MWh in March, 191.78 €/MWh in April, 187.14 €/MWh in May. The price in June was not uploaded so it was decided taking an average of the ones before: 215.66 €/MWh in June. The consumed electricity is shown in the table below, along with the resulting cost, to help you understand the actual cost in euros.

Equipment	Power Consumed (W)	Time (hours)	Electricity price (€/MWh)	Total Cost (€)
Laptop	50	Feb 120 h	200.47	1.20
		Mar 120 h	283.26	1.70
		April 120 h	191.78	1.15
		May 120 h	187.14	1.12
		June 120 h	215.66	1.29
Light	20	Feb 120 h	200.47	0.48
		Mar 120 h	283.26	0.68
		April 120 h	191.78	0.46
		May 120 h	187.14	0.45
		June 120 h	215.66	0.52
Ventilation	300	June 110 h	215.66	7.11
			Total	**16.16 €**

***Table 24**: Energy cost of use of the facilities.*

6.5. Total costs

Following the cost segmentation, the endeavour's overall budget is calculated by adding up each subtotal. This must consider an increase in overhead of 15% and an increase in project-related industrial benefit of 7%. The overheads are all the costs required to cover the payroll for the staff members that oversee the infrastructure but do not work on the project. This framework would take into account the license and server managers who made it possible to run simulations using GT-Suite, as well as the staff members responsible for the project's administrative side. The profit this initiative may indicate if it had a direct business interest is the industrial advantage, on the other hand.

Value-added taxes (VAT, or IVA in Spanish) of 21 % must be applied to the entire cost, bringing it to **4,674.76 €.**

References

ACEA. (2021). *Heavy-duty vehicles: Charging and refuelling infrastructure requirements.* European Automobile Manufacturers Association.

ACEA. (2022, April 2). *ACEA Driving mobility for Europe*. Retrieved from ACEA Driving mobility for Europe: https://www.acea.auto/figure/average-age-of-eu-motor-vehicle-fleet-by-vehicle-type/

Agency, I. E. (2019). *The Future of Hydrogen.* International Energy Agency.

BALLARD. (2016). *Product Data Sheet - FCMove-HD.*

BALLARD. (2016). *Product Data Sheet - FCVelocity-MD.*

BALLARD. (2021, August). *BALLARD.* Retrieved from https://www.ballard.com/markets/truck

Barbir, F. (2013). *PEM FCs: Theory and Practice.* Elsevier.

Bessie Noll, S. d. (2021). *Analyzing the competitiveness of low-carbon drive-technologies in road-freight: A total cost of ownership analysis in Europe.* Elsevier.

Claire Buysse, J. M. (2021). *The role of the European Union's vehicle CO2 standards in achieving the European Green Deal.* ICCT.

Coalition, E. (2010). *Fleet Electrification Roadmap: REVOLUTIONIZING TRANSPORTATION AND ACHIEVING ENERGY SECURITY.* Electrification Coalition.

Coalition, E. (2020). *Electrifying Freight: Pathways to accelerating transition.* Electrification Coalition.

Company, M. &. (2021). *Hydrogen Insights. A perspective on hydrogen investment, market development and cost competitiveness.* EU: Hydrogen Council.

Dario Bezmalinovic, B. S. (2015). Characterization of PEM FC degradation by polarization change curves. *Journal of Power Sources*, 82-87.

Desantes, J. N.-J. (2022). *Impact of the Powertrain Sizing on Cradle-to-Grave Emissions and FC Degradation in a FCV with a Range-Extender Architecture.* SAE Technical Paper.

DoE. (n.d.). Retrieved from DoE: https://www.hydrogen.energy.gov/pdfs/review18/st001_ahluwalia_2018_o.pdf

Dominik Murschenhofer, D. K. (2018). *A real-time capable quasi-2D proton exchange membrane FC model.* Elsevier.

Dutta, M. N. (2010). Effects of Upper Potential Dwell Time, Transients and Relative Humidity on PEM FC Cathode Catalyst Degradation.". *The Electrochemical Society*.

ENERGY.GOV. (n.d.). Retrieved from Office of Energy Efficiency & Renewable Energy: https://www.energy.gov/eere/fuelcells/hydrogen-fuel-basics

Eurostat. (2022). *Eurostat Statistics Explained*. Retrieved from Eurostat Statistics Explained: https://ec.europa.eu/eurostat/statistics-explained/index.php?title=Electricity_price_statistics

GaBi. (n.d.). Retrieved from https://gabi.sphera.com/solutions/product-carbon-footprint/

GREET. (n.d.). Retrieved from https://greet.es.anl.gov/

Guardiola C, P. B.-R. (2014). *A stochastic method for the energy management in hybrid electric vehicles. .* Elsevier.

H2Accelerate. (2021, August 24). Retrieved from https://h2accelerate.eu/

Huan Li, A. R. (2019). *Online adaptive equivalent consumption minimization strategy for FC hybrid electric vehicle considering power sources degradation.* Elsevier.

Hyundai Truck and Bus. (n.d.). Retrieved from Hyundai Truck and Bus: https://trucknbus.hyundai.com/global/en/products/truck/xcient-fuel-cell

IEA. (2019). *International Energy Agency*. Retrieved from International Energy Agency: https://www.iea.org/commentaries/the-clean-hydrogen-future-has-already-begun

IEA. (2021). *Tracking Transport.* International Energy Agency .

IPCC. (2012, August 5). Managing the Risks of Extreme Events and Disasters to Advance Climate Change Adaptation. *Cambridge University Press*.

J.M. Desantes, R. N.-J. (2022). *Effect of dynamic and operational restrictions in the energy management strategy on FC range extender electric vehicle performance and durability in driving conditions.* Elsevier.

K. H. Kangasniemi, D. A. (2004). Characterization of Vulcan Electrochemically Oxidized under Simulated PEM FC Conditions. *Journal of The Electrochemical Society*, 151 E125.

Kobunshi. (2008). *Polymer electrolyte FC.*

Luján JM, G. C. (2016). *Cost of ownership-efficient hybrid electric vehicle powertrain sizing for multi-scenario driving cycles. .*

Luján JM, G. C. (2019). *Optimal control of a turbocharged direct injection diesel engine by direct method optimization.* Elsevier.

McKinsey&Company. (2021). *Hydrogen Insights: A perspective on hydrogen investment, market development and cost competitiveness.* Hydrogen Council.

Nengyou Jia, M. D. (2009). Voltage Degradation Associated with Operational Conditions: Upper Potential and Lower Potential Limits. *The Electrochemical Society*.

Novella, R. (2020). *Comparative global warming impact and NOX emissions of conventional and hydrogen automotive propulsion systems.* Elsevier.

Novella, R. (2021). *A modeling framework for predicting the effect of the operating conditions and component sizing on FC degradation and performance for automotive applications.* Elsevier.

Novella, R. (2021). *Optimization and sizing of a FC range extender vehicle for passenger car applications in driving cycle conditions .* Elsevier.

Onori S, S. L. (2016). *Hybrid electric vehicles: Energy management strategies.* Elsevier.

P. Corbo, F. M. (2007). *Experimental analysis and management issues of a hydrogen FC system for stationary and mobile application,.* Elsevier.

P. Corbo, F. M. (2008). *Experimental analysis of a 20 kWe PEM FC system in dynamic conditions representative of automotive applications.* Elsevier.

Pier Giuseppe Anselma, G. B. (2021). *FC electrified propulsion systems for long-haul heavy-duty trucks: present and future cost-oriented sizing.* Applied Energy.

Pucheng Pei, Q. C. (2008). A quick evaluating method for automotive FC lifetime. *International Journal of Hydrogen Energy*, Pages 3829-3836.

S.Knights. (2012). 6 - Operation and durability of low temperature FCs. In S.Knights, *Polymer Electrolyte Membrane and Direct Methanol FC Technology* (pp. 137-177). Woodhead Plublishing.

Serrao L, O. S. (2009). *ECMS as a realization of Pontryagin's minimum principle for HEV control.* IEEE.

Shiyue Mao, H. B.-L. (2021). *TOTAL COST OF OWNERSHIP FOR HEAVY TRUCKS IN CHINA: BATTERY-ELECTRIC, FC ELECTRIC, AND DIESEL TRUCKS.* ICCT.

Teng T, Z. X. (2020). *A comprehensive review of energy management optimization strategies for FC passenger vehicle.* Elsevier.

Teng T, Z. X. (2020). *A comprehensive review of energy management optimization strategies for FC passenger vehicle.* Int J Hydrogen Energy.

The International Council on Transport. (2021, April 9). Retrieved from https://theicct.org/transport-could-burn-up-the-eus-entire-carbon-budget

Transport & Enviroment. (2022, February). Retrieved from https://www.transportenvironment.org/wp-content/uploads/2022/02/2022_02_TE_HDV_CO2_consultation_response_final.pdf

UK, V. T. (n.d.). *VOLVO TRUCKS UK*. Retrieved from VOLVO TRUCKS UK: https://www.volvotrucks.co.uk/en-gb/trucks/alternative-fuels/environmental-footprint-calculator/footprint-calculator.html?lang=en&market=gb&view=single&trucks=fh_2021&ucategories=longhaul,regional

Undertaking, C. H. (2019). *Hydrogen Roadmap Europe .* European Union.

Yvonne Ruf, M. B. (2020). *FCs Hydrogen Trucks.* FCs and Hydrogen Joint Undertaken.